

Plenary Lectures

PL1

INTERNAL STRESS REDISTRIBUTION DURING FATIGUE CRACK GROWTH IN LONG FIBRE METAL MATRIX COMPOSITES

P.J. Withers

Henry Royce Institute, Department of Materials, University of Manchester, United Kingdom
P.J.Withers@manchester.ac.uk

Unidirectional metal matrix composites have been under development since the 1960's but their application has been relatively modest. Nevertheless, they can offer extremely good properties in the reinforcement direction. In this talk I will focus in particular on Ti and Al-SiC monofilament composites which offer excellent strength to weight ratio at room and elevated temperature with potential applications within the aerospace and space domains [1].

Critical to their fatigue behaviour [2] is the manner in which stresses redistribute during fatigue crack growth. If the interface between fibre and matrix is too strong then the load at the crack tip is transferred locally to the reinforcing fibres and the fibres fracture. Too weak and the cracks will by-pass the fibres such that the fibres can bridge the crack but the composite will have poor mechanical properties especially in the transverse direction. The thermal residual stresses are also important because these determine the matrix clamping stresses which affect the fictional sliding stresses that occur as fibres are pulled out in the crack bridging region.

Synchrotron X-ray computed tomography can provide a detailed picture of the crack growth process and the fibre fractures. Diffraction is the only practical way in which the load transfer between the matrix and reinforcement can be mapped as a function of crack growth. Because it is phase selective diffraction allows the stress fields in both matrix and fibres to be mapped, the interface stresses between matrix and fibres inferred and the crack bridging stresses quantified [3, 4, 5].

In this talk I will examine how the thermal residual stresses, the frictional sliding stresses and the crack bridging stresses can be determined and show how these can explain the variation in crack tip growth rates as a function of fatigue crack growth. I will compare the behaviours for systems with fibres that are strongly bonded with those having sliding interfaces and look at how the internal

stresses vary as a function of service temperature [6,7]. Furthermore, this work illustrates the value of being able to combine imaging and residual stress measurements to quantify the effect of damage on internal stress redistribution.

1. Winstone, M.R., A. Partridge and J.W. Brooks, The contribution of advanced high-temperature materials to future aero-engines. Proceedings of the Institution of Mechanical Engineers Part L-Journal of Materials-Design and Applications, (2001). **215**: p. 63-73.
2. Cotterill, P.J. and P. Bowen, Fatigue crack growth in a fibre-reinforced Ti MMC at ambient and elevated temperatures. *Composites*, (1993). **12**, 214-221.
3. Hung, Y.-C., J.A. Bennett, M.D. Michiel, J.-Y. Buffière, T.J.A. Doel, P. Bowen and P.J. Withers, Fatigue crack growth and load redistribution in Ti/SiC composites observed in situ. *Acta Mater.*, (2009). **57**: 590-599.
4. Withers, P.J., Fracture mechanics by three-dimensional crack-tip synchrotron X-ray microscopy. *Philosophical Transactions of the Royal Society A-Mathematical Physical and Engineering Sciences* (2015). **373**: 20130157.
5. Wang, Y., et al., Damage accumulation during high temperature fatigue of Ti/SiCf metal matrix composites under different stress amplitudes. *Acta Materialia*, (2021). **213**, 116976.
6. Hung, Y.-C. and P.J. Withers, Fibre bridging during high temperature fatigue crack growth in Ti/SiC composites. *Acta Materialia*, (2012). **60**, 958-971.
7. Withers, P.J., J.A. Bennett and M. Kuroda, Interfacial shear strength behaviour of Ti/SiC metal matrix composites at room and elevated temperature. *Acta Mater.*, 2010. **58**: p. 6090-6103.



PL2

IMAGING STRAIN AND DEFECTS IN NANOCRYSTALS USING *IN SITU* BRAGG COHERENT DIFFRACTION IMAGING

M.-I. Richard^{1,2}, S. Labat³, M. Dupraz^{1,2}, S. Yeyha^{1,3,4}, C. Chatelier^{1,2}, C. Atlan^{1,2}, E. Bellec², N. Li^{1,2}, M. Grimes^{1,2}, A. Zakaria³, K. Olson^{1,2}, D. Simonne^{1,3}, T.U. Schüllli², E. Rabkin⁵, O. Thomas³, J. Eymery¹, F. Maillard⁶, S. Leake²

¹Université Grenoble Alpes, CEA Grenoble, IRIG, MEM, NRX, F-38000 Grenoble, France

²ESRF - The European Synchrotron, F-38000 Grenoble, France

³Aix Marseille Université, CNRS, Univ. Toulon, IM2NP UMR 7334, 13397 Marseille, France

⁴Synchrotron SOLEIL, Orme des Merisiers, 91190 Saint-Aubin, France

⁵Technion-Israel Institute of Technology, 3200003, Haifa, Israel

⁶Univ. Grenoble Alpes, Univ. Savoie Mont Blanc, CNRS, Grenoble INP, LEPMI, 38000 Grenoble, France. mrichard@esrf.fr

At the nanoscale, the properties of materials are largely influenced by elastic strain and depend critically on the presence of crystal defects. However, imaging and characterising the structure of defects inside a crystal in three-dimensions (3D) and *in situ* during reaction remain a challenge. The advent of the new 4th generation X-ray light sources represents an unprecedented opportunity to conduct *in situ* studies on the structure of nanoparticles during their operation. Here, we will illustrate how Bragg coherent x-ray imaging allows to image in 3D and at the nanoscale the strain and defect dynamics inside nanoparticles during heat treatment, catalytic reactions or nano-indentation. The technique appears, nowadays, as a revolutionary tool to image defects and strain fields in 3D.

First, we have demonstrated that the technique allows to reveal in 3D the structure of defects in Platinum (Pt) nanocrystals (NCs) and their associated lattice strains. Dislocations are characterised from their characteristic displacement and strain fields (see Figure 1). We also succeeded to reveal in 3D the detwinning process in a single Pt nanoparticle during *in situ* gas reaction. From the lattice displacement, the local strain of metal NCs can be examined *in situ* and *operando* during catalyst-enhanced reactions. This has been applied to Pt NPs under CO reaction conditions in the steady state to compare the strain changes at different facets. We have also successfully im-

aged the morphology, the lattice displacement and the strain of an individual Pt nanoparticle in electrochemical environment. The Bragg coherent x-ray imaging experiment can also be combined with a custom-built atomic force microscope to perform *in situ* mechanical testing. The 3D reconstructions from the Pt **111** coherent diffraction patterns allow the direct observation of the strain field inside the Pt particle during indentation and clearly show the nucleation of several dislocation arms beneath the AFM-tip that mostly lay in {111} planes (see Figure 2). Furthermore, multiple-Bragg reflections were recorded on the same particle to determine the full 3D strain tensor.

This imaging technique can be coupled with molecular statics simulations to investigate the 3D strain and stress fields in nanoparticles. We will also discuss the possibility to enable extremely high-resolution and high-energy imaging with Bragg coherent X-ray diffraction. Finally, we will highlight the potential of machine learning to predict characteristic structural features in nanocrystals just from their 3D Bragg coherent diffraction patterns.

In situ and non-invasive structural characterisation of defects during reaction opens new avenues for understanding defect behaviors in confined crystals and paves the way for strain and defect engineering.

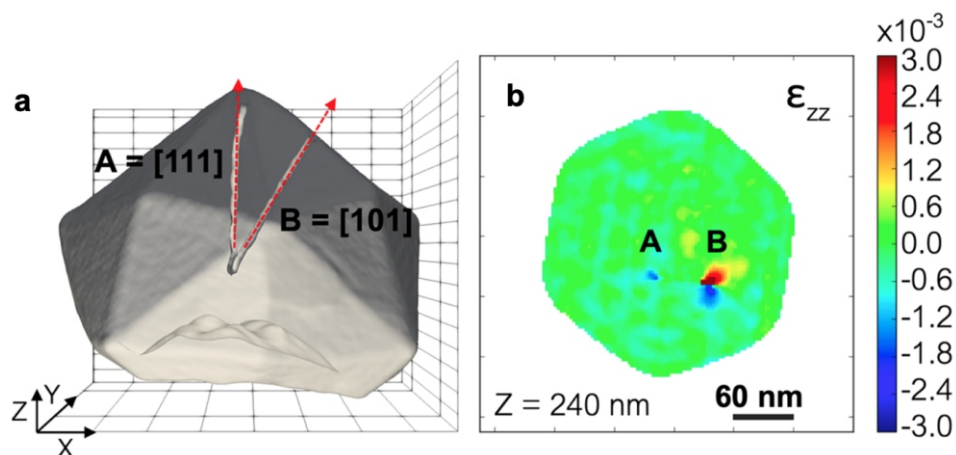


Figure 1. (a) Wireframe plots of the reconstructed electron density of a Pt particle drawn at 35% of the maximum density. A dislocation loop is evidenced. (b) Two-dimensional cut of the out-of-plane strain, ϵ_{zz} , at a particle height of 240 nm.

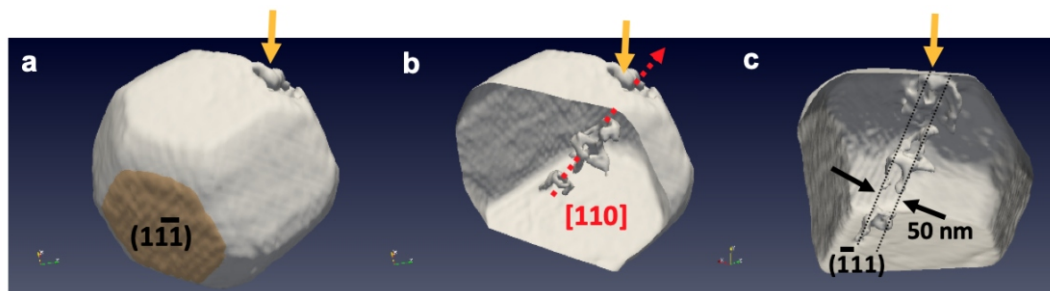


Figure 2. (a) 3D imaging of a 400 nm Pt nanocrystal during nanoindentation. (b) Dislocation network at the onset of plasticity (c) Identification of glide planes and dislocation loops size.

We acknowledge funding from the European Research Council (ERC) under the European Union's Horizon 2020 research and innovation programme (grant agreement No. 818823).

1. Robinson, I. & Harder, R. Coherent X-ray diffraction imaging of strain at the nanoscale. *Nat. Mater.* **8**, 291-298 (2009).
2. Richard, M.-I. et al. Anomalous Glide Plane in Platinum Nano- and Microcrystals. *ACS Nano* **17**, 6113-6120 (2023).
3. Carnis, J. et al. Twin boundary migration in an individual platinum nanocrystal during catalytic CO oxidation. *Nat. Commun.* **12**, 5385 (2021).
4. Dupraz, M. et al. Imaging the facet surface strain state of supported multi-faceted Pt nanoparticles during reaction. *Nat. Commun.* **13**, 3003 (2022).
5. Atlan, C. et al. Imaging the strain evolution of a platinum nanoparticle under electrochemical control. *Nat. Mater.* 1-8 (2023).
6. Dupraz, M. et al. 3D Imaging of a Dislocation Loop at the Onset of Plasticity in an Indented Nanocrystal. *Nano Lett.* **17**, 6696-6701 (2017).
7. Lim, B. et al. A convolutional neural network for defect classification in Bragg coherent X-ray diffraction. *Npj Comput. Mater.* **7**, 1-8 (2021).
8. Richard, M.-I. et al. Anomalous Glide Plane in Platinum Nano- and Microcrystals.

PL3

X-RAY RESIDUAL STRESS ANALYSIS THROUGH THE AGES: FROM LABORATORY TO SYNCHROTRON - AND BACK?

Ch. Genzel

Helmholtz-Zentrum für Materialien und Energie, Berlin, Germany
genzel@helmholtz-berlin.de

X-ray (residual) stress analysis (XSA) can reflect almost 100 years of tradition, the success of which is based on several features that characterize diffraction methods. They provide non-destructive and phase-selective information from different material zones with almost any resolution. Depending on the photon energy and the diffraction geometry, structure and property gradients can be analyzed from surface layers that are only a few nanometers thick down to the centimeter range in the volume of the material.

The lecture addresses the analysis of the residual stress state in the near-surface region of polycrystalline materials, which significantly influences the properties and lifetime of technical parts and components. This zone is characterized by the superposition of depth gradients, which include, for example, the chemical composition, the morphological and crystallographic texture, but also the elastic grain interaction between the crystallites or plastic deformation. Over the past decades, numerous XSA methods have been developed that focus on the treatment of one or more of the above-mentioned aspects [1, 2].

It is characteristic of the history of XSA (as of X-ray analysis in general) that methodological developments

were and are closely linked to technical developments in the field of increasingly powerful photon sources and detectors [3, 4]. Today, 3rd generation synchrotron storage rings allow experiments to be carried out with the highest spatial and time resolution. This enables, for example, the determination of residual stress distributions in sub-micrometer-thin sublayers of multilayer coatings [5] or the in-situ analysis of stress evolution during welding [6].

However, due to the very limited availability of beamtime at synchrotron beamlines, the development of high-performance, decentralized laboratory measurement stations is becoming increasingly important. In the lecture, it will be shown that the way from the synchrotron back to the lab does not just involve downscaling the experiments but necessitates advancements in methods and diffractometer hardware [7]. By removing the bottleneck in beamtime, XSA can be made accessible to a wider community. This appears particularly important for industry-driven materials research, as it often requires a quick response to new questions as well as the investigation of large sample series as part of process control.



1. I. C. Noyan & J. B. Cohen, *Residual Stress Measurement by Diffraction and Interpretation*. New York: Springer, 1987.
2. V. Hauk, *Structural and Residual Stress Analysis by Non-destructive Methods*. Amsterdam: Elsevier, 1997.
3. E. J. Mittemeijer & U. Welzel (eds.), *Modern Diffraction Methods*. Weinheim: Wiley-VCH, 2013.
4. P. Staron, A. Schreyer, H. Clemens & S. Mayer (eds.), *Neutrons and Synchrotron Radiation in Engineering Materials Science*. Weinheim: Wiley-VCH, 2017.
5. J. Keckes, R. Daniel, J. Todt, J. Zalesak, B. Sartory, S. Braun, J. Gluch, M. Rosenthal, M. Burghammer, C. Mitterer, S. Niese, A. Kubec, *Acta Mat.*, **144** (2018), 862.
6. Ch. Genzel, M. Klaus, N. Hempel, Th. Nitschke-Pagel, K. Pantleon, *J. Appl. Cryst.* **56** (2023), 526.
7. Ch. Genzel, M. Meixner, D. Apel, M. Boin, M. Klaus, J. Appl. Cryst. **54** (2021), 32.

PL4

INTERPLAY BETWEEN THE RESIDUAL STRESS AND MICROSTRUCTURE FEATURES

D. Rafaja

*Institute of Materials Science, TU Bergakademie Freiberg, Gustav Zeuner Street 5,
D-09599 Freiberg, Germany
rafaja@iww.tu-freiberg.de*

X-ray diffraction (XRD) is a well-established experimental technique for non-destructive analysis of residual stresses in crystalline materials. The residual stress analysis using XRD benefits mainly from the high resolution of XRD in the reciprocal space and consequently from a high precision of the lattice deformations determined from the changes of the interplanar spacing. As XRD concludes the lattice deformations from the change of the interplanar spacing, the lattice deformation can be precisely quantified for selected crystallographic directions (hkl) and for selected directions in the direct space that are related to the sample coordinates and that are typically described by angles and in a spherical coordinate system [1]. Moreover, XRD can distinguish lattice deformations occurring on different length scales, as they affect different characteristics of the diffraction lines like their positions, widths and shape.

A principal drawback of the X-ray residual stress analysis is that it cannot measure stresses directly. The stresses must be calculated from the measured lattice deformations using the elasticity theory and the generalized Hooke law taking the crystallographic anisotropy of the elastic constants into account [1]. In polycrystalline materials, X-ray elastic constants (XECs) are applied instead of the elasticity tensors of single crystals in order to consider the interactions between neighbouring grains having different orientations. For calculation of the XECs from the single-crystal elastic constants, the micromechanical models proposed by Voigt [2], Reuss [3], Neerfeld & Hill [4, 5], Eshelby & Kröner [6, 7], and Vook & Witt [8] are typically used. The capabilities of these models were discussed in detail in [9]. A generalized approach for description of the relationship between the measured lattice deformation and the residual stress was developed by Hauk & Dölle [10, 11], who introduced the stress factors that are capable of describing observed dependence of the lattice deformation on the crystallographic (hkl) and direct-space directions (φ , ψ) for textured samples. In materials containing crystal structure defects, the measured interplanar spacing can ad-

ditionally be affected by the presence of such defects and by their interaction with other microstructure features. An example of the microstructure defects that modify the interplanar spacing are planar defects, in particular stacking faults [12, 13].

In this contribution, the effect of the interplay of the microstructure features on the measured interplanar spacings and lattice deformation will be illustrated on the example of thermodynamically metastable austenitic steels showing the transformation-induced and/or twinning-induced plasticity (TRIP/TWIP) effect [14, 15]. The plasticity of these steels is enabled by the formation of perfect dislocations in the fcc austenite, their dissociation into partial dislocations, formation of stacking faults and their widening [16]. During a further plastic deformation of the TRIP/TWIP steels, the density of stacking faults increases, which facilitates the formation of ordered sequences of stacking faults that is followed by the phase transition of fcc austenite to hcp -martensite and to bcc ' -martensite, or by the formation of nanotwins.

The XRD experiments performed within this study were carried out *in situ* under deformation, both on a laboratory diffractometer and on a high-energy synchrotron source (PETRA III @ DESY, beamline P07). The information content of the combination of XRD and mechanical testing will be discussed. Furthermore, it will be shown how the interplay of the microstructure features affects the stress factors and how the effects observed in the XRD patterns can be used for identification of the individual processes during the plastic deformation and phase transitions and for the constitutive modelling [17]. The benefits of the holistic microstructure analysis using high-energy synchrotron radiation and the XRD operating in the transmission mode will be illustrated on a high coverage of the reciprocal and orientation space, which is made possible by a wide range of the diffraction vector, by a large variety of accessible hkl 's and by a broad accessible range of the sample orientations (φ , ψ) with respect to the deformation force.



1. I. C. Noyan & J. B. Cohen, *Residual Stress. Measurement by Diffraction and Interpretation*. New York: Springer. 1987.
2. W. Voigt, *Lehrbuch der Kristallphysik*. Leipzig: Teubner. 1910.
3. A. Reuss, *Z. Angew. Math. Mech.*, **9**, (1929), 49.
4. H. Neerfeld, *Mitt. K.-Wilh.-Inst. Eisenforsch.*, **24**, (1942), 61.
5. R. Hill, *Proc. Phys. Soc. London*, **65**, (1952), 349.
6. J. D. Eshelby, *Proc. R. Soc. A*, **241**, (1957), 376.
7. E. Kröner, *Z. Physik*, **151**, (1958), 504.
8. R. W. Vook, F. Witt, *J. Appl. Phys.*, **7**, (1965), 2169.
9. U. Welzel, J. Ligot, P. Lamparter, A. C. Vermeulen, E. J. Mittemeijer, *J. Appl. Cryst.*, **38**, (2005), 1.
10. H. Dölle, V. Hauk, *Z. Metallkd.*, **69**, (1978), 410.
11. H. Dölle, V. Hauk, *Z. Metallkd.*, **70**, (1979), 682.
12. B. E. Warren, *X-Ray Diffraction*, Dover Publications: Dover Books on Physics. 2012.
13. R. Kužel, R. Černý, V. Valvoda, M. Blomberg, M. Merisalo, *Thin Solid Films*, **247**, (1994), 64.
14. V. F. Zackay, E. R. Parker, D. Fahr, R. Busch, *Trans. ASM*, **60**, (1967), 252.
15. G. B. Olson, M. Azrin, *Metal. Trans. A*, **9**, (1978), 713.
16. D. Rafaja, C. Ullrich, M. Motylenko, S. Martin, *Springer Series in Materials Science*, **298**, (2020), 325.
17. S. Martin, A. Weidner, C. Ullrich, C. Schimpf, M. Motylenko, R. Lehnert, H. Biermann, D. Rafaja, A. Vinogradov, Y. Estrin, *Mater. Charact.*, **184**, (2022), 111667.



Keynote Lectures

KL1

SIMULTANEOUS NEUTRON AND X-RAY DIFFRACTION MEASUREMENTS OF STRAIN

P. J. Bouchard¹, A. Sprauel², S. Paddea¹, B. Tafazzoli¹, J. Kelleher³

¹Stress-Space Ltd., Atlas Building R27, Harwell Campus, Didcot, Oxfordshire OX11 0QX, UK

²Mesures Rayons X, 6 rue de Dingolfing, 67170 BRUMATH, France

³ISIS Pulsed Neutron & Muon Source, Harwell Campus, Didcot, Oxfordshire OX11 0QX, UK
john.bouchard@stress-space.com

Surface residual stresses in crystalline materials have been measured by laboratory X-Ray Diffraction (XRD) for 80 years or more and residual stresses deep within a material have been measured by neutron diffraction for around 40 years by using the atomic lattice planes as a strain gauge. This paper describes a Proof of Concept (PoC) project that has demonstrated, for the first time, measurement of deep strains in an engineering sample by neutron diffraction using the ENGIN-X instrument (ISIS Neutron and Muon Source) at the same time as measurement of surface residual strains in the same sample by X-ray diffraction. The opportunity for exploring this kind of dual measurement arose following the launch of new robotic XRD equipment (the “X-Raybot” developed MRX-Rays) guided by a laser vision system (a Stress-Space innovation) that facilitates accurate measurement positioning across the surface of complex geometry engineering components. The greatest challenge of the project was to avoid physical collisions between the X-Raybot (and its associated cabling) with ENGIN-X infrastructure and in particular the neutron de-

tectors. Following a feasibility study the X-Raybot was mounted on a purpose built stable platform behind the ENGIN-X positioning table. This gave the X-Raybot head access to the top surface of engineering samples mounted on the ENGIN-X table and facilitated simultaneous surface stress measurements along the diagonals (-45° to $+45^\circ$), that is in the same directions as being measured by neutrons. It also allowed surface areas of large engineering components up to 200 mm above the neutron gauge volume centre to be measured at the same time. A simple demonstration experiment was performed where the mean coefficient of thermal expansion (CTE) of A508 Class 3 steel for temperatures up to 230°C was successfully determined from surface X-ray diffraction lattice plane spacing measurements and simultaneous neutron diffraction bulk lattice parameter measurements of adjacent material with -45° and $+45^\circ$ alignments. The CTE measurements compare favourably with each other and published properties at temperatures above 100°C .

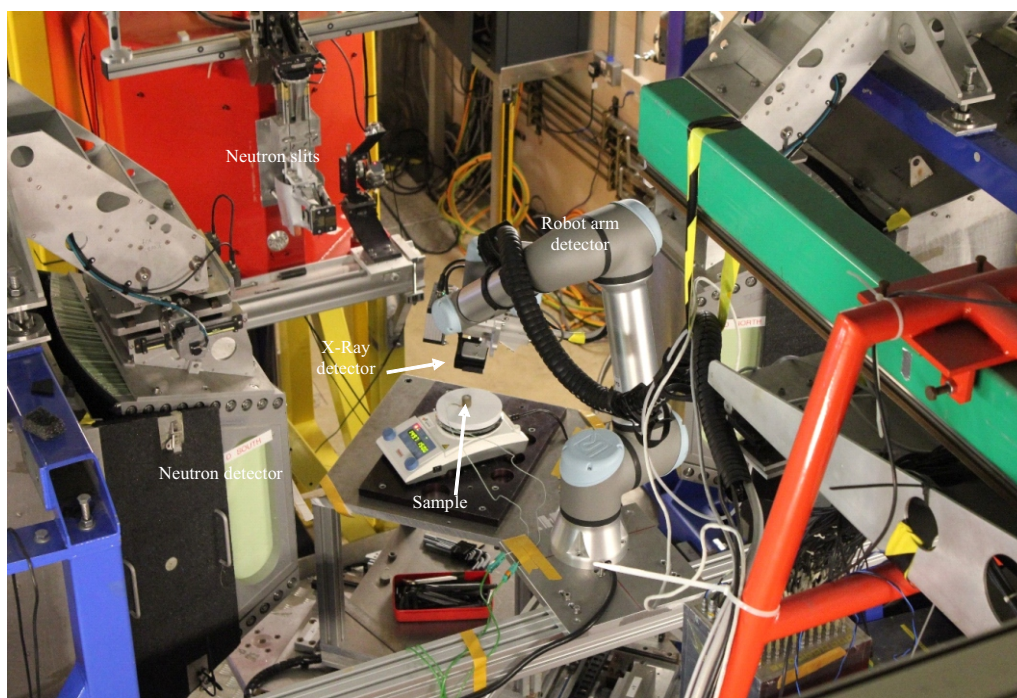


Figure 1. X-Raybot installed on ENGIN-X neutron instrument

KL2

MULTI-SCALE CHARACTERIZATION OF RESIDUAL STRESSES IN SPENT AGR FUEL CLADDING

X. van Heule^{1*}, C. Truman¹, H. Coules¹, R. Clark²

¹University of Bristol, Queen's Building, University Walk, Bristol, BS8 1TR, UK

²National Nuclear Laboratory Ltd, 102B Stonehouse Park, Sperry Way, Stonehouse, GL10 3UT, UK
xavier.vanheule@bristol.ac.uk

Under the aqueous conditions of the long-term wet storage of spent Advanced Gas-cooled Reactor (AGR) fuel pins, Stress Corrosion Cracking (SCC) poses a risk to the structural integrity of the cladding. The driving force behind this SCC is believed to be a tensile residual stress state within the cladding. There is currently no information about the magnitude and distribution of these residual stresses, and as a result, it is unclear what fraction of the pins is affected. At present, commercially available residual stress measurement techniques are not applicable to spent AGR fuel pins, mainly due to radiological and geometrical constraints. As a result, in this work, the adaption of various techniques for application on AGR fuel was investigated.

In relation to SCC, the length scale of the mechanical stresses is an important criterion to factor into the selection of the measurement techniques. Clear evidence exists of a macroscopic threshold stress before the onset of SCC, and, beyond this threshold, crack growth rates have been observed to increase proportionally with the magnitude of the stress. Therefore, the first technique which was investigated was one at the macro-scale, being Incremental Centre Hole Drilling (ICHD). ICHD was selected since it yields all three in-plane stress tensor components, while only inflicting limited damage to the sample. Furthermore, initial analysis showed good feasibility for its application on AGR fuel cladding. On the other hand, more recently, the microscopic phenomena governing SCC at the length scale of individual grains have been subjected to increased scrutiny as well. For this purpose, a second technique capable of measuring stresses at this length scale was investigated as well, being micro-Hole Drilling (μHD). Finally, X-Ray Diffraction was used as an independent validation measurement for the two other techniques.

For the application of ICHD on AGR fuel cladding, firstly, bespoke calibration data was determined using Finite Element Analysis (FEA). Secondly, the classical strain gauge rosettes used with ICHD were not compatible with the cladding either, therefore Digital Image Correlation (DIC) was investigated as an alternative means for measuring strain. Consequently, an experimental rig to combine ICHD and DIC was designed and built as well. This rig was then used to measure the stresses in externally loaded samples of AGR fuel cladding, validating the process. Then, to demonstrate the feasibility of the technique in a relevant environment as well, a prototype for remotely performing combined ICHD and DIC measurements on AGR fuel pins inside a hot cell was designed and built. Finally, this prototype was tested in a mock-up hot cell on cold samples, serving as a relevant environment without the risks involved with highly radioactive samples.

Moving on to the micro-scale, with μHD, a Focused Ion Beam (FIB) is used to mill microscopic trenches to relax stresses similarly as with ICHD. Images captured using a Scanning Electron Microscope (SEM) are analysed with DIC to measure the strain relaxation. For the current study, a sample extracted from an unirradiated AGR fuel cladding tube was subjected Electron Back-Scatter Diffraction (EBSD) prior to μHD. This allowed the targeting of specific grains, taking into account their orientation and grain boundary properties. The measured stresses could then be correlated with these microstructural properties.

This work was funded by the Nuclear Decommissioning Authority (NDA) through the NDA Bursary Scheme. Additional funding was provided by EPSRC and NDA for the design, construction, and testing of the ICHD-DIC prototype.



KL3

DARK FIELD X-RAY MICROSCOPY: A NEW WAY OF 4D MAPPING OF STRAIN AND ORIENTATION OF EMBEDDED CRYSTALLINE STRUCTURES

Can Yildirim^{1*}, Henning. F. Poulsen², Hugh Simons², Raquel Rodriguez-Lamas¹,
Albert Zelenika^{1,2}, and Carsten Detlefs¹

¹ European Synchrotron Radiation Facility, 71 Avenue des Martyrs, 38043 Grenoble Cedex 9, France

² Department of Physics, Technical University of Denmark, 2800 Kgs. Lyngby, Denmark

*can.yildirim@esrf.fr

Macroscopic physical and mechanical properties of many technological materials are determined by their hierarchically-organized structures such as grains, domains, and defects. These structures span over length scales ranging from nanometers to millimeters. Understanding the interplay between these length scales is of critical importance not only for improving material properties but also for validation of multi-scale models. Here, we present Dark Field X-ray Microscopy (DFXM), a diffraction-based synchrotron method for probing 3D nanostructures with their associated strain and orientation in bulk materials. Analogous to dark-field electron microscopy, DFXM comprises an objective lens to magnify diffracting features from millimeter-sized samples [1-2]. The resulting spatial and angular resolutions are on the order of 100 nm and 0.001°, respectively. DFXM is a full field imaging technique. This allows for recording 3D strain and orientation maps of the

entire heterogeneity in a given grain within seconds to minutes, thus capturing time-resolved phenomena. The microscope can be coupled with coarser grain mapping methods such as 3DXRD and Diffraction Contrast Tomography (DCT) without having to dismount the sample. Here, we demonstrate the microstructure-property relationships in metal alloys such as steel, aluminum, and nickel along with functional oxides and semiconductor materials using DFXM [1-4].

1. Kutsal et al., IOP Conf. Series: Materials Science and Engineering, 2019, 580, 012007.
2. Simons et al., *Nature Communications*, 2015, 6, 6098.
3. Yildirim et al., *MRS Bulletin*, 2020, 45, 277.
4. Yildirim, et al, *Scripta Materialia*, 2022, 214, 114689.

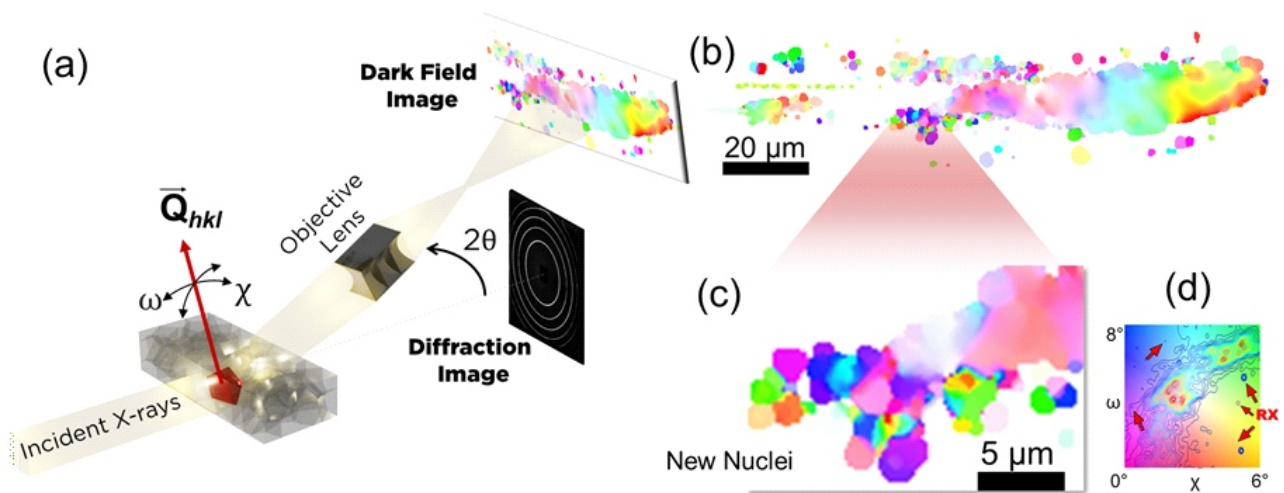


Figure 1. a) Schematics of DFXM. A monochromatic beam with photon energies ranging from 15 to 33 keV illuminates the sample. An embedded structural element (i.e. grain) is aligned such that the beam is diffracted. The diffracted beam is focused using an objective and an image is projected on to a detector located at 5 meters away from the sample. (b) Reconstructed cross-sectional DFXM local orientation map of an embedded grain of interest in a partially recrystallized 85% cold-rolled Fe-3%Si-0.1%Sn alloy. (c) Zoom in on recrystallized grain in relation to retained (non-recrystallized) deformed grain. (d) Color key showing the local orientation with an overlaid contour map of the integrated intensity distribution, adopted from [4].

MULTI-SCALE MECHANICAL BEHAVIOUR OF CARBURIZED AUSTENITIC STAINLESS STEELS CLADDING FOR THE NEW GENERATION OF SODIUM-COOLED FAST NUCLEAR REACTORS

M. F. Slim¹, J. P. Goulmy¹, G. Geandier², M. Lamari³, F. Rouillard⁴, B. Malard⁵, L. Barrallier¹

¹Arts et Métiers Institute of Technology, MSMP, F-13617 Aix-en-Provence, France

²Université de Lorraine, CNRS, IJL F-54000 Nancy, France

³MINES Paritech, PSL University, MAT – Centre des matériaux, CNRS UMR 7633, BP 87 91003 Evry, France

⁴Université Paris-Saclay, CEA, Service de recherche en Corrosion et Comportement des Matériaux (S2CM), 91191, Gif-sur-Yvette, France

⁵CIRIMAT, Université de Toulouse, CNRS, INPT, 4 Allée Émile Monso, 31030 Toulouse, France
mohamed-fares.slim@ensam.eu

In the new generation of sodium-cooled fast nuclear reactors (SFR), the neutron fission rate is controlled with B₄C pellets encapsulated in austenitic stainless-steel cladding. Feedbacks from first tests in former French experimental sodium fast reactors evidenced the premature failure of this cladding. From the expertise of the broken cladding, it has been demonstrated that the carburization of the austenitic stainless-steel (ASS) cladding, due to interaction with sodium and B₄C pellets at temperatures between 500 °C and 600 °C, was the main cause of failure. From previous studies [1 – 4], it has been shown that after exposure to carburizing liquid sodium: i) a highly carburized zone developed within the samples, ii) depending on the temperature, the carbon that has diffused into the steel oversaturated the austenitic matrix or formed carbides. Moreover, titanium-stabilized austenitic stainless steel (Ti-ASS) and solution annealed 316L alloys that have been studied showed different carbon concentration profiles and carbide volume fractions within the depth of the samples [1, 2]. The developed microstructure led to the formation of layers with different mechanical properties giving the ASS cladding a mechanical behaviour similar to that of a composite material. To our knowledge, the mechanical behaviour of these ASS carburized in nuclear industry has been only studied at the macroscopic scale [5, 6]. The objective of this study is to carry out a comprehensive investigation of the evolution of the mechanical behaviour of Ti-ASS and 316L after exposure to liquid sodium at 500 °C for 1000 h.

The carbon concentration profile within the depth of the samples was measured using electron probe micro-analyzer (EPMA). Microhardness measurements were carried out on the cross section of the samples at initial state and after carburization. In-situ tensile tests combined with high energy X-ray diffraction (HEXRD) and Digital Image Correlation (DIC) were conducted at the Petra P21.2 Swedish materials science beamline. A high energy monochromatic beam (E = 82.5 keV) with dimensions of 300 µm (H) × 10 µm (V) was used to probe the mechanical field gradient within the thickness of the samples. A 2D Varex detector placed at 1.4 m from the sample was used to record the whole Debye-Scherrer rings. The recorded 2D diffraction images were used to determine the profile of the phase fractions, stress gradient and stress partitioning between

the phases within the sample thickness at different loading steps. The fracture surfaces were characterized using scanning electron microscope (SEM).

The EPMA results showed a carbon profile gradient within the samples. The affected thicknesses in Ti-ASS and 316L alloys were equal to 140 µm and 180 µm respectively. At the surface of the Ti-ASS sample, the carbon concentration reached 1.5 wt. % while a higher carbon concentration, 3.1 wt. %, was measured at the surface of the 316L alloy. The HEXRD diffraction patterns collected on the 316L sample showed the formation of carbides within the first 70 µm of the surface. However, no carbides were detected within the carburized Ti-ASS. Microhardness measurements revealed a hardness increase within the affected thickness as compared to the initial state samples. The microhardness and phase fraction profiles showed a symmetrical behaviour as expected. The macroscopic tensile curves showed an evolution in the mechanical behaviour for both alloys. For 316L alloy, an increase in yield strength accompanied with a loss of ductility was observed. The Ti-ASS showed a different evolution, with almost no increase in yield strength, no loss of ductility and an increase in the failure stress. The XRD measurements revealed a stress field gradient across the sample thicknesses during loading. For the Ti-ASS, higher yield and failure stresses were observed in the affected zone. However, in the core of the sample, where tensile residual stresses were generated due to carburization [2, 3], the yield and failure stresses were lower than in the non-carburized alloy. The full width at half maximum (FWHM) of the XRD line profiles of the different phases at the surface of the carburized 316L alloy revealed decohesion between the carbide and the austenitic matrix. Therefore, brittle fracture occurred in the zone where carbides were present. In the carbide-free zone, the austenite matrix showed a ductile behaviour with an increase of the FWHM and continuity of stress rise. These observations are consistent with the fractography images observed on the 316L alloy.

1. M. F. Slim, G. Geandier, B. Malard, F. Rouillard, *Metalurgical and Materials Transactions. A*, **52**, 4438 – 4453, (2021).



2. M. F. Slim, G. Geandier, M. Romedenne, F. Rouillard, B. Malard, *Oxidation of Metals*, **96**, 185 – 199 (2021).
3. M. F. Slim, G. Geandier, F. Rouillard, B. Malard, *Acta Materialia*, **221**, 117435 (2021).
4. M. Romedenne, F. Rouillard, D. Hamon, B. Malard, D. Monceau, *Corrosion Science*, **159**, 108147 (2019).
5. J. L. Krankota, *Journal of Engineering Materials and Technology*, **98**, 9 – 16 (1976).
6. N. S. Baharasi, M. G. Pujar, C. R. Das, J. Philip, K. Thyagarajan, S. Paneerselvi, A. Moitra, S. Chandramouli,

V. Karki, S. Kannan, *Journal of Nuclear Materials*, **516**, 84 – 99 (2019).

The authors gratefully acknowledge the Deutsche Elektronen-Synchrotron (DESY-Petra III, Hamburg, Germany) for provision of beamtime at the PETRA P21.2 Swedish materials science beamline. We would like to thank all the beamline staff for the assistance during the experiments.

KL5

THE REPRODUCIBILITY OF RESIDUAL STRESS IN ADDITIVELY MANUFACTURED BENCHMARK SAMPLES AS MEASURED BY NEUTRON AND SYNCHROTRON X-RAY DIFFRACTION

R.C. Laurence¹, D. Canelo-Yubero², E. Maawad², G. Abreu Faria², P. Staron²,
R. Ramadhan^{3,4}, S. Cabeza³, A. Paecklar³, T. Pirling³, M. Sanchez-Poncela⁵,
R. Blanc⁶, E. Baustert⁶, P.J. Withers¹, M.J. Roy¹

¹Henry Royce Institute, University of Manchester, United Kingdom

²Helmholtz-Zentrum Hereon, Germany

³Institut Laue-Langevin (ILL), France

⁴ISIS Neutron and Muon Source, United Kingdom

⁵ArcelorMittal Global R&D, Spain

⁶Volum-e, France

Robin.laurence@manchester.ac.uk

Additive manufacturing typically generates significant residual stresses in manufactured parts as a result of exposure to repeated high thermal gradients during manufacturing as the laser scans over the part. This residual stress can be detrimental to the final properties or in extreme cases if the stress is high, the part will deform significantly when removed from the substrate. This study was aimed at better understand the issues associated with making reliable residual stress measurements by neutron and synchrotron diffraction. Neutron diffraction (SALSA at ILL [2]) and multiple synchrotron X-ray diffraction (SXR) beamlines (P07 and P61A at DESY, operated by Hereon [3]) were used to map the residual stress within four geometrically identical laser powder bed fusion (LPBF) additively manufactured 316L stainless steel arches. Two different manufacturing facilities each provided a pair of components, referred to as sets M1 and M2. Each facility used a differ-

ent substrate in terms of both dimensions and material properties. These sets were then measured both as-built and after identical stress relieving heat treatments. These components represent part of the EASI-STRESS round robin benchmarking of residual stress measurement techniques [4]. The geometry is shown in Fig. 1 consisting of a 20 mm square topped arch of height 10 mm. This shape induces an overhang in the printing process, which is a common challenge for LPBF additive manufacturing. The stress was measured by diffraction along a path extending from the top surface to the apex of the arch above the void at the midplane of the component.

Despite different processing conditions, the resultant stress state in the measured locations is similar for M1 and M2 (Fig. 2). Both sets are fully dense but made with different input volumetric energy densities and a different number of layers. For any given layer, the majority of the stress

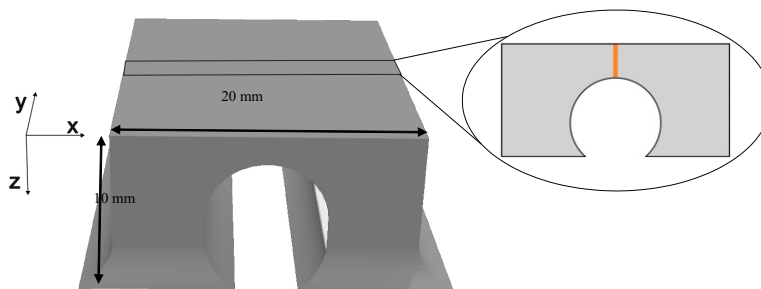


Figure 1. LPBF additively manufactured arch geometry and cross section view showing measurement path at the centre of the part in orange.

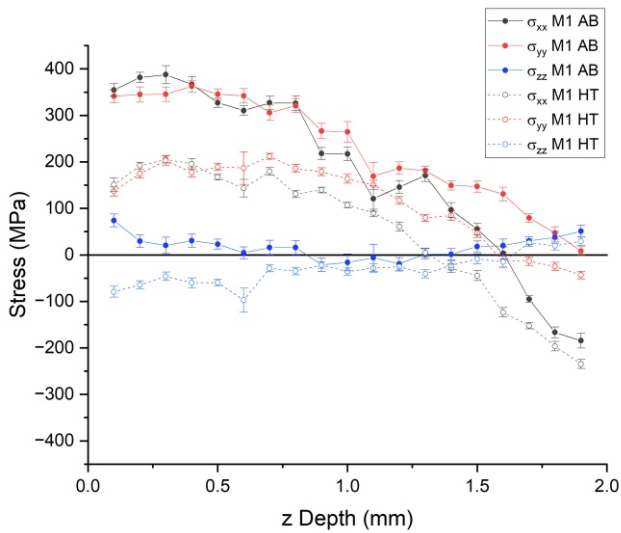


Figure 2a. Residual stress of the M1 part in the three principal directions both as built (AB) and after heat treatment (HT).

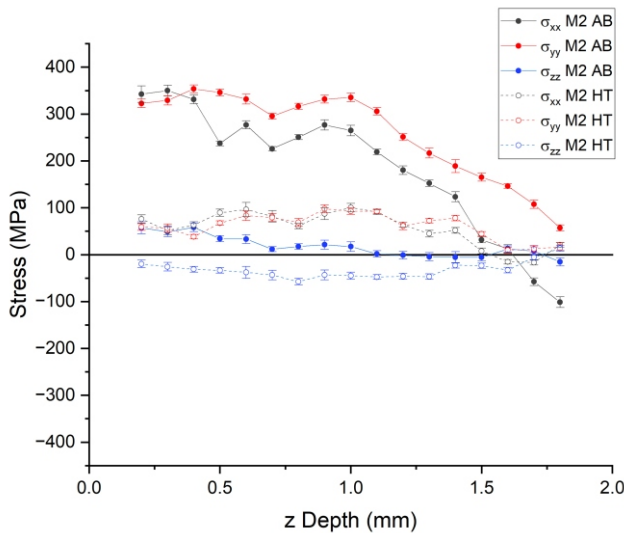


Figure 2b. Residual stress of the M2 part in the three principal directions both as built (AB) and after heat treatment (HT).

can only begin to be ‘locked in’ once the melt pool starts to solidify, the level of stress build up is therefore defined by the temperature difference between this solidification temperature and the temperature of the already built part and

substrate. Both manufacturing protocols had substrates preheated to the similar temperature, resulting in similar heat transfer conditions. The contributions of those parameters which are different between the two parts to the residual stress, such as any resultant temperature gradient [5], must be smaller and on the order of the measurement uncertainty for the techniques applied so cannot in this case be observed.

Fig. 2 also shows the stress in the two sets after a 2 hour 700 °C heat treatment in an inert atmosphere. Heat treatments are commonly applied to LPBF parts in an effort to reduce the residual stress arising from the manufacture [6]. In both sets the tensile stress in the x and y directions decreases appreciably. Despite both starting in the same stress state, the M2 part exhibits a larger reduction in stress, especially at the top surface, where it falls by 300 MPa as opposed to 200 MPa for M1. As the yield stress in the arch falls with increasing temperature, plastic deformation will occur in both arches resulting in a stress levelling effect. The increased stress reduction in the HT M2 part is driven by a misfit between the arch and the substrate caused by differences in the rate of thermal expansion. This misfit is much less significant in the HT M1 part.

This work shows that the residual stress within EASI-STRESS benchmark LPBF parts can be reliably determined by bulk diffraction techniques. The residual stress in such parts in the as-built condition is reproducible by different manufacturers and is not necessarily determined by the choice of processing parameters which produce a fully dense part. The heat treatment applied was shown to reduce the as-built tensile residual stress and the effectiveness of such heat treatments is seen to be influenced by the choice of substrate and deposition materials.

1. Mercelis, P. and Kruth, J.P., *Rapid Prototyping Journal*, **12**(5), (2006), 254-265.
2. Pirling, T., Bruno, G., and Withers, P. J., *Materials Science and Engineering: A*, **437**, (2006), 139-144.
3. Schell, N., et al., *Materials Science Forum*, **772**, (2014), 57-61.
4. Cui, W., et al., ICRS 11 - The 11th International Conference of Residual Stresses (2022).
5. Edwardson, S. P., Griffiths, J., Dearden, G., Watkins, K. G., *Physics Procedia* **5**, (2010), 53–63.
6. Williams, R.J., et al., *Journal of Manufacturing Processes*, **57**, (2020), 641-653.



KL6

BARKHAUSEN NOISE IN TERM OF STRESS STATE

M. Neslušan

Faculty of Mechanical Engineering, Univerzita 1, 01026 Žilina, Slovakia
Miroslav.neslusan@fstroj.uniza.sk

This presentation is dealing with magnetic Barkhausen noise and the role of stresses in this physical phenomenon. Ferromagnetic bodies contain domain substructure, when the neighbouring atoms within the domain are aligned in the same direction. The neighbouring magnetic domains are separated by domain walls. When the ferromagnetic body is exposed to the altering magnetic field, domain walls tend align along the direction of this magnetic field. However, their motion at low fields is reversible due to presence of pinning sites (lattice imperfections) and their displacement is on the short distance only. As soon as the magnetic field exceeds the critical threshold exceeding the critical pinning strength of pinning sites, irreversible motion in the form of Barkhausen jumps occur. Domain walls in such case produce electromagnetic as well as acoustic pulses which can be detected on the free surface. Interaction of domain walls with pinning sites mean that Barkhausen noise contains information about microstructure [1]. On the other hand, Barkhausen noise is also a function of stress state when domains and the corresponding domain walls align along the direction of tensile stresses which in turn increases the amplitude of Barkhausen noise pulses. In the case of compressive stresses, domain walls are aligned in the direction perpendicular against the direction of the compression which in turn decreases Barkhausen noise. The aforementioned evolution is valid for Fe alloys due to its positive magnetostriction whereas in the case of Ni and its ferromagnetic alloys the evolution is reversed [2].

Evolution of Barkhausen noise along with stresses and sensitivity of this technique with respect of non-destructive

monitoring is driven by the competition between the energy of magneto crystalline anisotropy and magneto elastic energy. As soon as the magneto elastic energy prevails, the evolution between Barkhausen noise and stress state saturates. It can be reported that the influence of residual stresses with respect of Barkhausen noise in many cases (especially when the density of lattice defects is high) is weak and microstructure dominates. Sensitivity of Barkhausen noise with respect of stresses measured in-situ of for example uniaxial tensile test or compression, bending, etc. is good. However early saturation can be found and surface corrosion or/and the initial microstructure heterogeneity produced during components manufacturing makes employment of Barkhausen noise technique for assessment of stress quite difficult task. This presentation contains case studies in which Barkhausen noise is investigated in term of stress state. Provided relationships were obtained during laboratory measurements on the model materials together with the real industrial application in the bearing and automotive industry as well as civil engineering.

1. B.D. Cullity, C.D. Graham, *Introduction to the magnetic materials*. New Jersey: IEEE Press. 2009.
2. S. Chikazumi, *Physics of ferromagnetism*. Oxford: Oxford University Press. 2005.

This work was realized within the frame of the project VEGA project 1/0052/22.

KL7

SIMULTANEOUS IMPROVEMENT OF FATIGUE STRENGTH AND BIOCOMPATIBILITY OF Ti-6Al-4V BY LOW-ENERGY LASER PEENING

K. Akita¹, Y. Iino¹, K. Sugiyama¹, A. Momozawa², Y. Sano^{3,4}, Y. Mizuta³, S. Tamaki³, and T. Shobu⁵

¹Department of Mechanical Systems Engineering, Faculty of Science and Engineering, Tokyo City University, 1-28-1 Tamazutsumi, Setagaya-ku, Tokyo 158-8557, Japan

²Department of Medical Engineering, Faculty of Science and Engineering, Tokyo City University, 1-28-1 Tamazutsumi, Setagaya-ku, Tokyo 158-8557, Japan

³Department of Quantum Beam Physics, SANKEN, Osaka University, 8-1 Mihogaoka, Ibaraki 567-0047, Japan

⁴Institute for Molecular Science, National Institutes of Natural Sciences, 38 Nishigo-Naka, Myodaiji, Okazaki 444-8585, Japan

⁵Materials Sciences Research Center, Japan Atomic Energy Agency, Tokai, Ibaraki 319-1195, Japan
akitak@tcu.ac.jp

Laser peening (LP) has been applied to relatively large mechanical components and structures, such as turbine blades and nuclear reactor welds, for improving fatigue strength and preventing stress corrosion cracking, because LP can introduce deeper residual stresses than other mechanical surface treatment techniques. One other unique feature of LP is the precise controllability of the laser irradiation conditions including laser energy, pulse width, spot diameter, pulse density. Therefore, LP has excellent applicability to localized areas and small components. In particular, the low-energy LPwC utilizing recently developed low-energy and short-pulse laser sources [1] is considered to be highly applicable to small components. In the low-energy LPwC, a low-energy laser source with a laser energy of a few mJ, which is about one-hundredth that of conventional laser peening is used. Even with a low laser energy, the peak power density which is a measure of the pressure of plasma shock wave become sufficiently high by reducing the laser spot diameter and the pulse width, thus enabling the generation of compressive residual stresses in the surface layer of metallic materials [2].

The authors are working on improving the fatigue properties of small components using the low-energy LPwC. One of the applications is dental and surgical implants. Titanium alloys are mainly used for the load-bearing parts of implants. Both of fatigue strength and biocompatibility are important factors for the implant design, however, it is difficult to reconcile both. To improve the biocompatibility of titanium alloys, an appropriate surface roughness is required, and the surface roughness is introduced into the surface by surface treatment techniques, such as chemical etching, grit blasting, and oxidizing. However, these surface treatments often lead to a reduction in fatigue strength [3]. In the present study, we revealed that the low-energy LPwC can improve both the fatigue strength and biocompatibility of a titanium alloy, simultaneously.

Figure 1 shows the axial strain distributions along the diameter axis of Ti-6Al-4V round bar specimens with a diameter of 5 mm and 3 mm that were treated by a conventional LP (200 mJ) [4] and the low-energy LPwC (1.5 mJ and 6.3 mJ), respectively. Sufficiently high compressive residual strains about 5000×10^{-6} were introduced on the

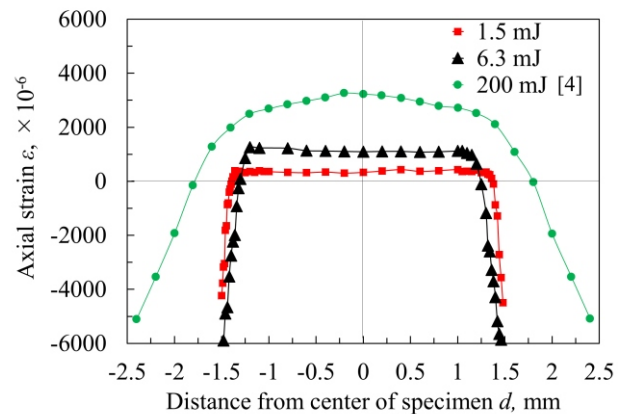


Figure 1. Axial strain distributions along the diameter axis of laser peened Ti-6Al-4V round bar specimens measured at SPring-8/BL22XU.

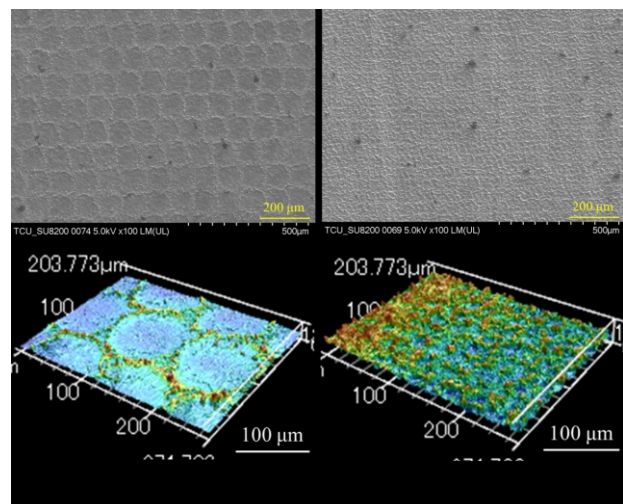


Figure 2. SEM (upper) and laser microscope (lower) images of Ti-6Al-4V treated by the low-energy LPwC with laser energy of 1.5 mJ.

surface layer for both specimens. Whereas the balancing tensile strains inside the specimens were quite different, there was large tension in the conventional LP specimen even though the specimen was thicker than the low-energy



LPwC specimens. The large tension is due to the deep compression in small specimens, which can induce internal crack initiation and short fatigue lives [4]. On the other hand, the surface compression was large and the balancing tension inside was very small in the low-energy LPwC specimen as shown in Fig. 1, therefore, surface crack initiation was suppressed, and early internal cracking was avoided. As a result, the fatigue limit of the low-energy LPwC specimens are improved about 20% against that of the non-LP specimens.

Biocompatibility in implants, which means the bonding between bone tissue and implant surface (namely, osseointegration), is as important as fatigue strength. Appropriate surface roughness for the osseointegration is about a few micrometres. Figure 2 (a) and (b) show the surface morphologies of Ti-6Al-4V treated by the low-energy LPwC with laser pulse density of 100 and 1600 pls/mm², respectively. The surface texture was changed regularly with laser condition, and the surface roughness was around 1.0-1.2 micrometres. Cell culture tests on these specimens were conducted using mouse osteoblast cell line, MC3T3-E1 and cell culture medium, -MEM+FBS (10%). The test results showed favourable osseointegration. Although the mechanism of osseointegration is not fully understood, it is

considered that not only surface roughness but also its microscopic shape influences the process. Considering that LP also possesses control over surface microscopic shape, further improvements in osseointegration performance can be expected by optimizing the LP condition.

The above results show that the fatigue strength and biocompatibility of Ti-6Al-4V can be improved simultaneously in a single laser peening process.

1. Y. Sano, *Metals*, **10**, (2020), 152.
2. Y. Sano, K. Masaki, Y. Mizuta, S. Tamaki, T. Hosokai, and T. Taira, *Metals*, **11**, (2021), 1716.
3. C. Leinenbach and D. Eifler, *Biomaterials*, **27**, (2006), 1200.
4. K. Masaki, Y. Kameshima, N. Hisamori, Y. Sano, K. Akita, T. Shobu, *J. Soc. Mater. Sci., Jpn.*, **62**, (2013), 297.

The authors thank Mr. Reiji Sakata of Kamijima Heat Treatment Co., Ltd. for preparing samples. A part of this study was supported by MEXT KAKENHI Grant Number JP20K04185 and JST-MIRAI Program Grant Number JPMJMI17A1. The synchrotron radiation experiments were performed at the BL22XU of SPring-8 with the approval of the Japan Synchrotron Radiation Research Institute (JASRI) (Proposal No. 2022B3726).

KL8

EVOLUTION OF STRESS FIELDS DURING CRACK GROWTH AND ARREST IN MICRO-CANTILEVERS DURING *IN SITU* BENDING ASSESSED BY CROSS-SECTIONAL X-RAY NANODIFFRACTION

Michael Meindlhumer¹, Markus Alfreider¹, Manfred Burghammer², Martin Rosenthal², Rostislav Daniel¹, Anton Hohenwarter¹, Christian Mitterer¹, Juraj Todt¹, Daniel Kiener¹ and Jozef Keckes¹

¹Department of Materials Science, Montanuniversität Leoben, Franz Josef Straße 18, 8700 Leoben, Austria

²ESRF, The European Synchrotron, 71 Avenue des Martyrs, CS40220, 38043 Grenoble Cedex 9, France
michael.meindlhumer@unileoben.ac.at

In order to improve our understanding of the fracture behaviour in nanocrystalline micro-cantilevers, it is necessary to elucidate the multiaxial stress and strain fields throughout their irreversible deformation, especially in the regime where simplified homogeneous linear elastic assumptions are not valid anymore. In this work, cross-sectional X-ray nanodiffraction (CSnanoXRD) with a spatial resolution of 200 nm was coupled with an *in situ* indentation device to uncover the multi-axial strain fields associated with crack growth. Here, (i) a notched clamped cantilever prepared from a multi-layered thin film composed of four alternating brittle CrN and semi-ductile Cr layers on high-speed steel and (ii) a freestanding cantilever fabricated from a high-pressure torsion processed nanocrystalline FeCrMnNiCo alloy were *in situ* stepwise loaded. Both cantilevers were manufactured by consecutive femto-second laser ablation and focused ion beam milling.

The Cr/CrN clamped cantilever was loaded stepwise to 150 and 460 mN and multi-axial stress distributions were retrieved in a region of interest of 40 × 30 μm². An effective negative stress intensity of -5.9±0.4MPa m^{1/2} accompa-

nied by a plastic zone extending up to 1.4 μm around the notch tip arose in the notched Cr sublayer as a consequence of residual stress in the thin film. The *in situ* experiment indicated a strong influence of the residual stresses on the cross-sectional stress fields evolution and crack arrest capability at the CrN-Cr interface. In detail, crack growth in the notched Cr layer to the adjacent CrN-Cr interface occurred at a critical stress intensity of 2.8±0.5MPa m^{1/2}.

The freestanding FeCrMnNiCo cantilever was loaded to 22, 45 and 34 mN loads, which corresponds to conditions where elastic loading, crack tip blunting and void formation and coalescence with the crack front are the governing mechanisms, respectively. In that case, CSnanoXRD data were evaluated in a region of 30 × 35 μm² centered around the crack tip. At a load of 22 mN, a bending stress up to ~±1 GPa was evaluated, while directly in front of the notch the crack opening stress raised to ~4 GPa. In a 200 nm circular zone around the notch the measured stress distributions deviated evidently from the linear-elastic fracture mechanics assumptions. At 45 mN, crack opening stresses increased to ~4.5 GPa and up to 1 μm from the crack tip a distinct plastic zone formed.

Further loading lead to a breakdown of the commonly assumed crack tip singularity and a significant decrease of the evaluated stress magnitude.

The quantitative experimental stress results provide unprecedented insights into the gradual stress evolution at the

crack tip and across the cantilevers as well as associated fracture processes in nanocrystalline materials.

KL9

MICRO- AND NANOMECHANICAL *IN-SITU* INVESTIGATIONS OF DISTINCT INTERFACES

M. Burtscher¹, M. Alfreider¹, C. Gammer², D. Kiener¹

¹Department of Materials Science, Montanuniversität Leoben, Franz-Josef Straße 18, 8700 Leoben, Austria

²Erich Schmid Institute of Materials Science, Austrian Academy of Sciences (ÖAW), Jahnstraße 12, 8700 Leoben, Austria

michael.burtscher@unileoben.ac.at

In situ micro- and nano-mechanical investigations are a powerful tool to elucidate deformation condition, residual stress state and fracture mechanical processes. Being direction-dependent and applicable to small sample volumes, these measurements provide mechanical parameters for different interfaces. Imaging techniques can also be used to record the prevailing deformation and fracture processes and gain insights through post-processing. Secured mechanical parameters are crucial for predicting component lifetime and ensuring safety in various applications. To achieve this, it is important to consider the same length scale and magnitude of the prevailing mechanisms. By using different specimen preparation approaches, it is possible to reach various length scales and design specimens that comply with the prevailing loads. These methods are gaining increasing attention in the materials science community.

This presentation will discuss various techniques for preparing micro- and nanomechanical specimens. To prepare micro-mechanical specimens, a femtosecond laser can be used to quickly remove vast amounts of sample material with minimal impact on the specimen surface [1]. By applying a smart pattern, repeatable specimen types can be easily achieved, and the time required for finishing by focused ion beam microscopy (FIB) can be minimized (see Figure 1). To avoid potential size effects, which are common at this length scale, it is vital to use different specimen sizes [2,3]. The synergetic effect of these methods is crucial for preparing specimens at various length scales.

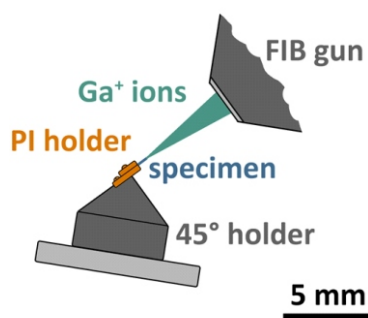


Figure 1. Sketch of specimen fabrication via FIB.

While miniaturized deformation and fracture experiments are becoming increasingly common, residual stresses in thin films are commonly measured using wafer curvature measurements or X-ray diffraction. However, these methods only provide an average of the global stresses. To reveal the residual stresses along or within individual thin film layers, a smart specimen design, local material removal, and *in-situ* methods can be used [4]. Therefore, the deflection of the remaining bending beam is used to continuously determine the prevailing residual stresses with a step size of approximately 50 nm [5].

Additionally, the mechanical properties of free-standing cantilevers can be determined using an indenter installed in a scanning electron microscope. Thereby, micro-mechanical spectroscopy can be used to determine the precise Young's modulus and damping capability of a confined volume [6]. Moreover, by introducing a notch in the specimen, it is possible to determine the fracture mechanical descriptors such as the fracture toughness, the J-integral, and the crack tip opening displacement through the evaluation of the mechanical response combined with computer vision techniques [7].

Similar deformation and fracture experiments can also be conducted using a transmission electron microscope. However, in this case, the specimen preparation is more delicate due to the significant decrease in length scale. Additionally, other factors such as electron transparency, removal of surface-sensitive FIB damage, and several other requirements must be met (see Figure 2). The responding force signal is also lower, ranging in the μN regime and subject to uncertainties arising from measurement physics. However, tracking the crack length provides access to the fracture toughness of different interfaces. This information is vital for systems that model macroscopic material behaviour or predict lifetime. Nano-beam diffraction can be implemented to record diffraction information for every point along the specimen. By determining the relative shift of these patterns, strains within the specimen and along specific interfaces can be measured with nanometer resolution [8]. An exemplary strain map of a lamellar interface is displayed in Figure 3. This can even be achieved during *in situ* fracture experiments by pausing the indenter and recording a strain map at relevant positions. From this data,

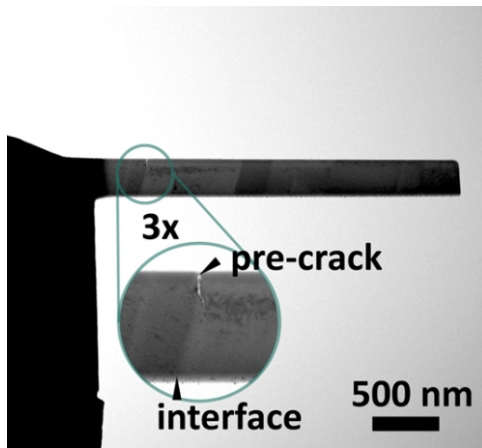


Figure 2. Finished cantilever in STEM mode.

detailed information on the deformation zone in front of the crack and dislocation interactions are accessible.

In conclusion, by merging different miniaturized testing techniques, a comprehensive understanding of the residual stress state, deformation and fracture behaviour of specific interfaces in engineering materials can be derived. This knowledge can in turn be used to tune the involved interfaces towards higher strength or ductility through alloying design. Therefore, micro- and nano-mechanical investigations offer numerous possibilities for the development of future smart responsive materials.

1. M.J. Pfeifenberger, M. Mangang, S. Wurster, J. Reiser, A. Hohenwarter, W. Pfleging, D. Kiener, R. Pippan, *Materials&Design*, 121, (2017), 109–118, <https://doi.org/10.1016/j.matdes.2017.02.012>.
2. J.R. Greer, J.T.M. De Hosson, *Progress Materials Science*, 56, (2011), 654–724. <https://doi.org/10.1016/j.pmatsci.2011.01.005>.
3. K. Schmuck, M. Burtscher, M. Alfreider, M. Wurmshuber, D. Kiener, *JOM*, EUROMAT23, (2023), <https://doi.org/10.1007/s11837-023-06348-7>.
4. R. Treml, D. Kozic, J. Zechner, X. Maeder, B. Sartory, H.-P. Gänser, R. Schöngrundner, J. Michler, R. Brunner, D. Kiener, *ActaMaterialia*, 103, (2016), 616–623. <https://doi.org/10.1016/j.actamat.2015.10.044>.
5. D. Kozic, R. Treml, R. Schöngrundner, R. Brunner, D. Kiener, T. Antretter, H.-P. Ganser, Evaluation of the Resid-

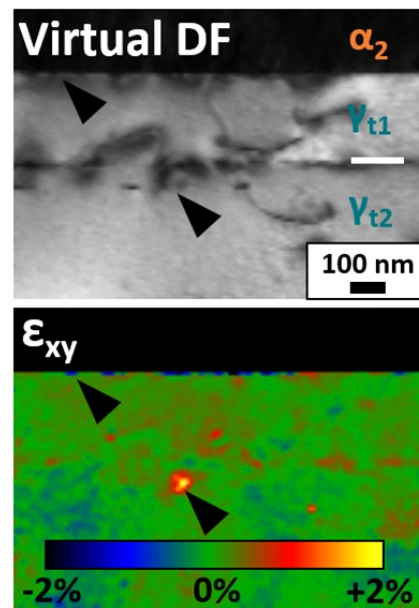


Figure 3. Recorded strain map of a lamellar structure.

ual Stress Distribution in Thin films by Means of the Ion Beam Layer Removal Method, *EuroSim*, (2014).

6. M. Alfreider, M. Meindlhumer, T. Ziegelwanger, R. Daniel, J. Keckes, D. Kiener, *MRSBulletin*, 49 (2023), 49–58, <https://doi.org/10.1557/s43577-023-00549-w>.
7. M. Burtscher, M. Alfreider, K. Schmuck, H. Clemens, S. Mayer, D. Kiener, *Journal Materials Research*, (2020), 1–14, <https://doi.org/10.1557/s43578-020-00088-z>.
8. I. Issa, C. Gammer, S. Kolitsch, A. Hohenwarter, P.J. Imrich, R. Pippan, D. Kiener, *MaterialsToday*. (2021), <https://doi.org/10.1016/j.mattod.2021.03.009>.

KL10

RESIDUAL STRESSES IN COLD-FORMED WELDED HIGH STRENGTH STEELS

Th. Nitschke-Pagel¹, M. Dadkhah¹, J. Gibmeier², M. Zürn²¹Institut für Füge- und Schweißtechnik, TU Braunschweig, Germany²Institut für angewandte Materialien, KIT, Germany

Low and high strength steels are widely used in the automotive industry for body car constructions. In order to avoid strength reduction and welding induced distortion a general understanding about the interaction of cold forming condition and the evolution of welding induced residual stress is of great practical importance.

Investigations have been carried out using different steel grades, a normalized S355MC, a high strength TRIP-steel HCT690T and a high strength TWIP-steel X40MnCrAlV 19 2.5 2. The residual stress evolution was investigated using XRD in welded joints with different cold forming conditions. The experimental investigations are supported by additional numerical simulations of the welding induced thermal cycles and residual stresses using the experimentally determined temperature dependent mechanical properties of the investigated steels and FEM-tools ABAQUS and SYSWELD.

The results reveal that the residual stress conditions depend strongly on the temperature cycles induced by the welding process. The resulting distributions of the residual

stresses depend on the interaction of the hindered shrinkage and the different microstructural changes in the welded zones.

Plastic deformations due to cold forming reduces the initial residual stresses in the low strength steel (S355MC) almost completely even at low plastic strains while the high strength steels show a more differentiated behaviour. The TRIP-steel shows a significant dependency between the heat cycle, the transformation behaviour in the cooling state, the incident and the remaining content of retained austenite while in the austenitic TWIP-steel the resulting residual stresses are mainly influenced by the high strengthening capacity in combination with the particular degree of plastic deformation. Therefore the residual stresses of the welds is not exclusively characterized by a strain induced residual stress relaxation but also by increasing residual stress magnitudes in the weld zones.

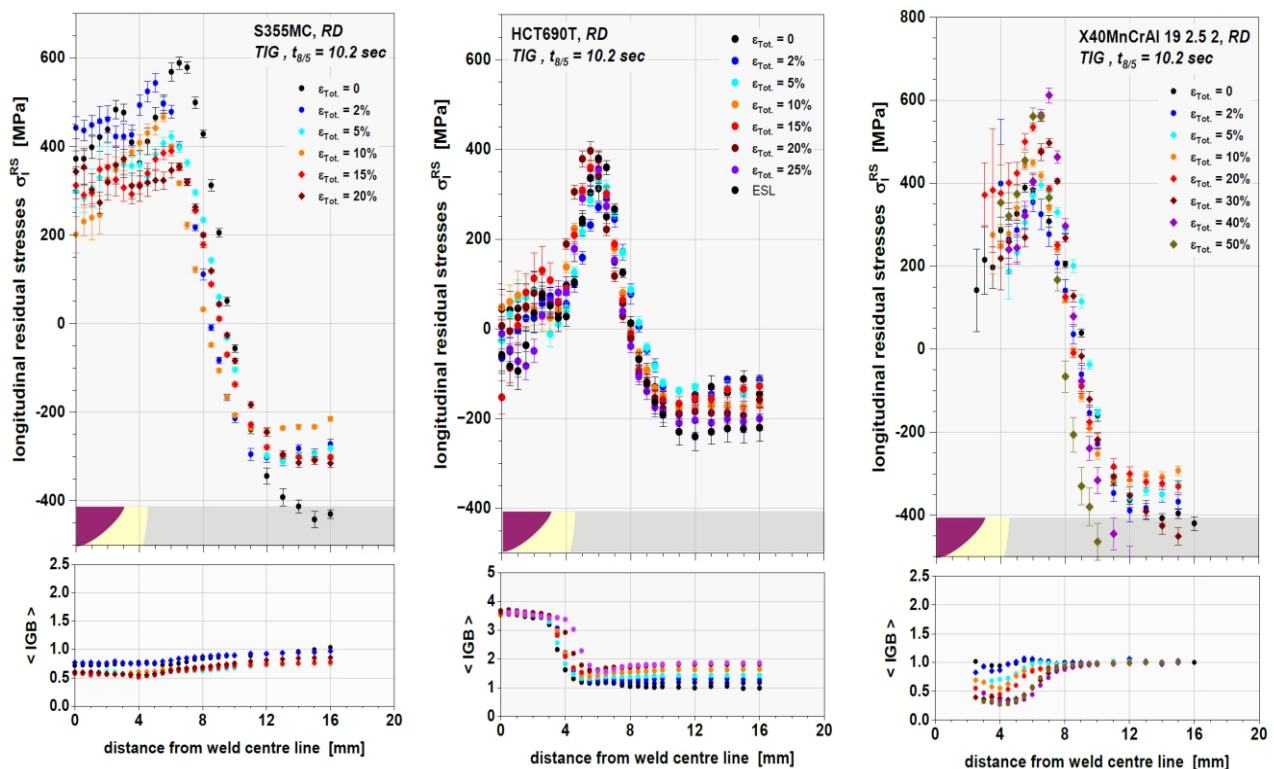


Figure 1. Comparison of the longitudinal residual stresses in different cold formed steels after TIG-welding.



KL11

X-RAY STRESS FACTORS IN DIFFRACTION STRESS ANALYSIS USED FOR INTERIOR AND SURFACE OF THE SAMPLE

A. Baczmański¹, M. Marciszko-Wiąckowska², Ch. Braham³, S. Wroński¹, M. Klaus⁴,
Ch. Genzel⁴

¹AGH University of Krakow, WFIS, al. Mickiewicza 30, 30-059 Krakow, Poland

²AGH University of Krakow, ACPIN, al. Mickiewicza 30, 30-059 Krakow, Poland

³Arts et M'etiers-ParisTech, PIMM, CNRS UMR 8006, 151 Bd de l'Hopital, 75013 Paris, France

⁴Abteilung für Mikrostruktur- und Eigenspannungsanalyse, Helmholtz-Zentrum Berlin für Materialien und Energie, Albert-Einstein-Str. 15, Berlin 12489, Germany
baczman@agh.edu.pl

The so-called Laplace space methods were applied to measure gradient of residual stresses RS in the subsurface layers of the sample. These techniques are based on the assumption that the information depth in reflection mode is defined by the absorption of the X-rays, which intensity decreases exponentially with the path length of the beam within the material. The choice of the measurement method and energy of radiation used, in general, depends on the material and the range of investigated depth; however, the data treatment strategy is also crucial. In the present work, two Laplace space techniques (ED and AD [1,2]) were applied to measure stress variation in the near-surface layers. On the other, the diffraction methods using high energy synchrotron radiations allowed us to measure lattice strains and to determine stress state in the interior of the sample.

To determine the stress tensor from the measured lattice strains the X-ray stress factors (XSF) must be used in analysis of measured lattice strains [3]. The XSFs can be determined from the experiment or calculated using theoretical models. The model applicability must be verified, especially for elastically anisotropic crystals and textured samples. In this work the in-depth evolution of elastic interactions of the grains was determined and used to calculate XSFs. The proper choice of grain interaction model

is necessary to carry out correct stress analysis, therefore in the present study, calculations of the XSFs were performed using three commonly used grain-interaction models (Reuss, Voigt, Eshelby-Kröner) and newly proposed “tunable Free-surface” model [4]. Then the obtained results were compared with different diffraction experiments in which the external load was applied and corresponding relative lattice strains were measured, moreover the elastic strains with respect to unloaded sample was determined. This way the influence of residual second order plastic incompatibility stresses [1,5] on the experimentally determined XSFs was minimized.

Results presented in this work were obtained for mechanically polished austenitic sample. The evolution between Free-surface (surface) and Eshelby-Kröner (bulk) was described by the exponential decrease of $r(z)$ parameter (where z is the depth below surface) expressing vanishing of grains interaction in the direction perpendicular to the free surface [4]. It was found that for the interior of the sample, the XSFs were correctly predicted by the Eshelby-Kröner model, and the rapid decrease of the $r(z)$ parameter starts at a depth (z) approximately equal to the mean grain size and $r(z)$ decreases to zero towards the sample surface (Fig. 1a). It means that one layer of grains is

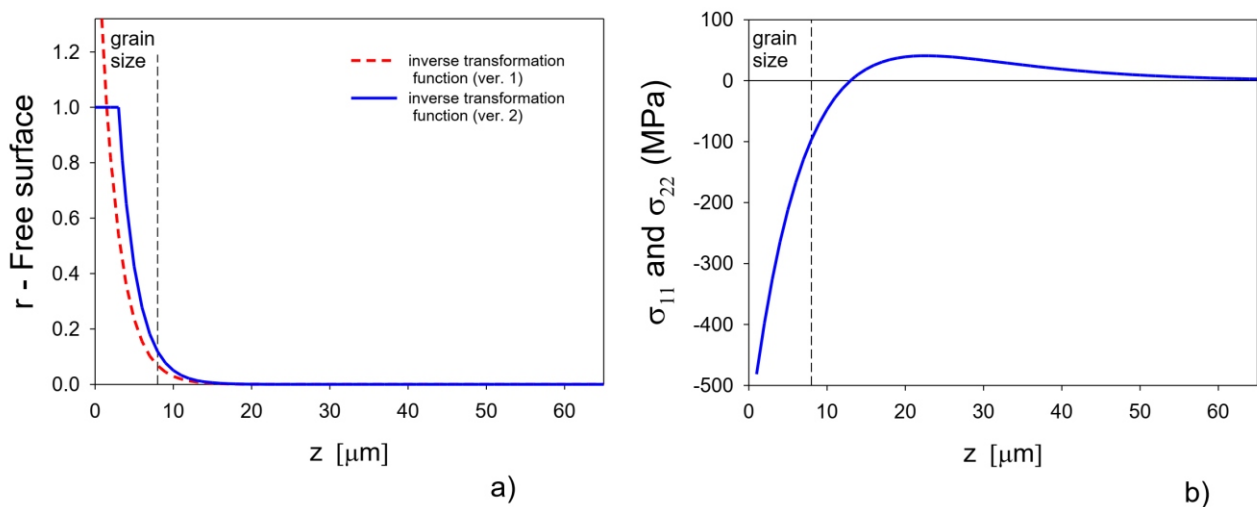


Fig. 1 The in-depth dependence of grain interaction (a), described by the r parameter (tunable free-surface model [4]) and stress σ_{11} and σ_{22} (b) in function of the real depth z below the surface. The results were obtained on the basis of different types of diffraction tests performed for mechanically polished austenitic sample.

enough to compensate for the free-surface effect, and under this layer the Kröner-Eshelby model correctly describes the interactions between grains. The relaxation of intergranular stress close to sample surface leads to good agreement of experimental results with free-surface model. Similar conclusions can be drawn when weighted Reuss-Voight model is considered, i.e. the Reuss model describes well the interaction of grains close to the surface, while the Kröner-Eshelby model is correct for depths greater than the average grain size [4]. Having values of XSFs the stress in-depth profile for mechanically polished austenitic sample was determined and presented in Fig. 1b.

1. M. Marciszko, A. Baczmanski, C. Braham, M. Wróbel, S. Wroński, G. Cios, *Acta Mater.* **123** (2017) 157–166.
2. M. Klaus, C. Genzel, *J Appl Cryst.* **46**, (2013), 1266–1276.
3. V. Hauk, *Structural and Residual Stress Analysis by Non-destructive Methods*, Elsevier, 1997.

KL12

ENERGY-DISPERSIVE X-RAY STRESS ANALYSIS IN PRESENCE OF RESIDUAL STRESS-, COMPOSITION- AND GRAIN INTERACTION DEPTH GRADIENTS

M. Klaus¹, Ch. Genzel¹, M. Marciszko-Wiąckowska², A. Baczmanski³

¹*Helmholtz-Zentrum für Materialien und Energie, Berlin, Germany*

²*AGH University of Krakow, ACPIN, Kraków, Poland*

³*AGH University of Krakow, WFiS, Kraków, Poland*
klaus@helmholtz-berlin.de

X-ray stress analysis (XSA) of polycrystalline materials is usually based on the assumption that the elastic grain interaction, which can be described by various models for calculating the diffraction elastic constants (DEC), is homogeneous and isotropic within the depth range covered by the X-ray beam. In this case, it is possible to determine the DEC model and the residual stress depth distribution simultaneously for materials with a cubic crystal structure using an optimization procedure [1]. However, as introduced in [2] and recently shown experimentally [3], there is evidence that at least a small surface layer may feature a different, anisotropic grain interaction behavior characterized by a free deformation of the crystallites in the surface normal direction and a constrained deformation parallel to it.

In this lecture, we address the question of the influence of depth-dependent grain interaction on XSA measurements performed in energy-dispersive (ED) diffraction mode through simulated case studies. For this purpose, the grain interaction in a certain surface layer is described by the direction-dependent Vook-Witt model [4], while the Eshelby-Kröner model [5, 6], which is isotropic at the macroscopic scale, is assumed in the bulk material. For various combinations of superimposed residual stress and composition depth gradients, $d^{hkl} \sin^2$ -distributions are calculated and analyzed using the modified multi-wavelength plot method (MMWP) [7] and the multi- hkl method [8], respectively.

Against the background of a depth dependency of the grain interaction, the results provide a differentiated pic-

4. M. Marciszko-Wiąckowska, A. Oponowicz, A. Baczmanski, Ch. Braham, M. Wątroba, M. Wróbel, M. Klaus, Ch. Genzel, *Measurement*, **194**, (2022), 111016.
5. M. Marciszko-Wiąckowska, A. Baczmanski, Ch. Braham, S. Wroński, R. Wawszczak, G. Gonzalez, P. Kot, M. Klaus, Ch. Genzel, *Materials Characterization*, 203 (2023), 113114.

1. *This work was financed by a grants from the National Science Centre, Poland (NCN), No. UMO-2021/41/N/ST5/00394 and No. UMO-2023/49/B/ST11/00774.*

2. *The research project was partly supported by the program "Excellence initiative – research university" for the AGH University of Science and Technology.*

Furthermore, we would like to thank Helmholtz-Zentrum Berlin für Materialien und Energie for the beamtime provided at 7T-MPW-EDDI beamline (BESSY II).

ture concerning the suitability of the two methods for separating residual stress and composition depth gradients. For both methods, the influence of a depth-dependent grain interaction can be suppressed if the respective evaluation primarily includes those reflections hkl with DEC close to the model-independent direction *. In contrast, a composition depth gradient has a significantly different effect on the analysis. Here, the integrating character of the MMWP method leads to systematic shifts in the depth profiles for both the residual stresses and the strain-free lattice parameter. In contrast, the multi- hkl method, which is based on the evaluation of sectional planes parallel to the surface, can correctly separate stress and composition gradients.

1. M. Klaus, Ch. Genzel, *J. Appl. Cryst.*, **52** (2019), 94.
2. A. Baczmanski, P. Lipinski, A. Tidu, K. Wierzbanski, B. Pathiraj, *J. Appl. Cryst.*, **41** (2008), 854.
3. M. Marciszko-Wiąckowska, A. Oponowicz, A. Baczmanski, Ch. Braham, M. Wątroba, M. Wróbel, M. Klaus, Ch. Genzel, *Measurement*, **194** (2022), 111016.
4. R. W. Vook, F. Witt, *J. Appl. Phys.* **36** (1965), 2169.
5. J. D. Eshelby, *Proc. R. Soc. London Ser. A*, **241** (1957), 376.
6. E. Kröner, *Z. Phys.* **151** (1958), 504.
7. Ch. Genzel, C. Stock, W. Reimers, *Mater. Sci. Eng. A*, **372** (2004), 28.
8. M. Klaus, Ch. Genzel, *J. Appl. Cryst.*, **50** (2017), 252.



KL13

MECHANISM OF SURFACE RESIDUAL STRESS GENERATION BY LASER PEENING AND INFLUENCE OF COEFFICIENT OF THERMAL EXPANSION

Y. Sano^{1,2}, K. Akita³

¹Department of Quantum Beam Physics, SANKEN, Osaka University, 8-1 Mihogaoka, Ibaraki 567-0047, Japan

²Institute for Molecular Science, National Institutes of Natural Sciences, 38 Nishigo-Naka, Myodaiji, Okazaki 444-8585, Japan

³Department of Mechanical Systems Engineering, Faculty of Science and Engineering, Tokyo City University, 1-28-1 Tamazutsumi, Setagaya-ku, Tokyo 158-8557, Japan
 yuji-sano@sanken.osaka-u.ac.jp

Laser peening (LP) is a well-known surface enhancement technique that induces favourable compressive residual stresses (RSs) by irradiating water-covered metallic materials with intense laser pulses [1]. Before LP is applied, an ablative layer is formed on the surface to prevent melting or damage from the intense laser pulse irradiation. This technique improves the fatigue properties of metallic components sufficiently so that LP entered real-world applications in the early 1990s such as reducing foreign object damage (FOD) in jet engine fan blades [2]. However, applications were limited to near-flat surfaces due to the difficulty of forming ablative layers on complex geometries.

The authors invented another type of LP called LPwC (laser peening without coating), which does not use ablative layers [3, 4]. LPwC can be used for complex 3D structures, such as gears and holes, because it only irradiates laser pulses onto bare surfaces. However, it seems inevitable that tensile RS will occur on the top surface due to shrinkage after laser pulse irradiation [5, 6], which poses another challenge to the realisation of LPwC: how to mitigate the thermal effects of direct laser pulse irradiation.

This study presents the detailed RS distribution around the laser-irradiated spot by means of synchrotron radiation and shows how compressive RS can be built up on the surface by successive laser pulse irradiation. Figure 1 shows the RS distribution obtained as a result of irradiating single or multiple laser pulses at the same location on the surface

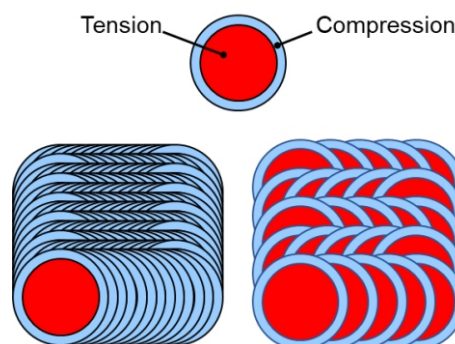


Figure 2. Overlap effect of laser pulses on RS.

of high-strength steel HT1000 [7]. Large tensile RSs remained within the laser spot, while compressive RSs were observed around the tensile region.

Figure 2 schematically shows the RS state after the single pulse irradiation (top) and after the successive laser pulse irradiations with dense and sparse overlap (bottom). The red area corresponds to the laser spot with tension, while the blue area is compressive and surrounds the laser spot. It can be expected that the successive laser pulses with sufficient overlap will erase the tensile area except for the last spot [7]. The change in surface RS due to the LPwC treatment with increasing overlap is plotted in Fig. 3, along with the depth profile of RS. By increasing the overlap, the top surface can be compressive despite the intense thermal effect of the laser pulse irradiation [5, 6].

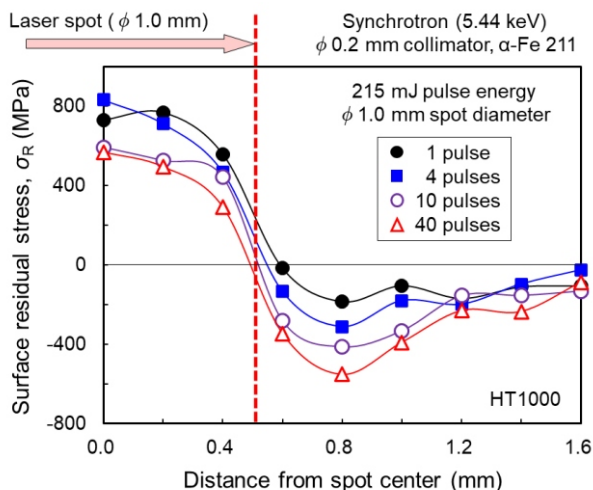


Figure 1. Surface RSs in and around laser spot.

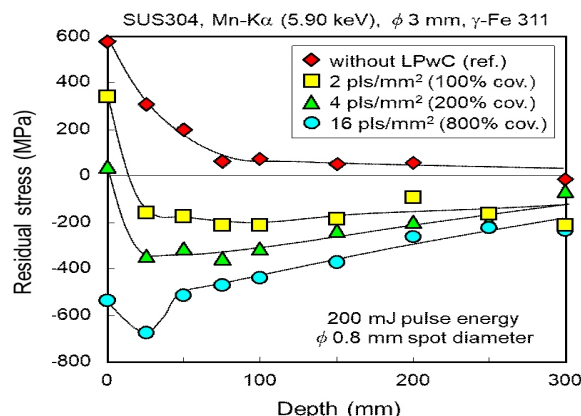


Figure 3. Overlap effect on RS of SUS304.

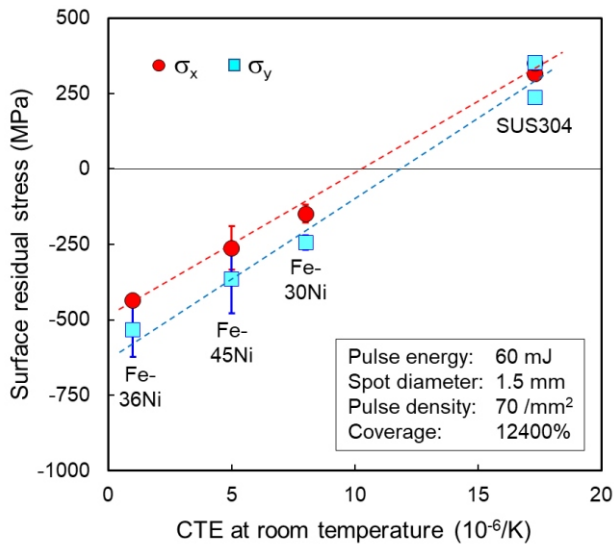


Figure 4. Relation between CTE and surface RS.

Roughly speaking, the surface RS is determined by the balance between the compressive component by the laser pulse and the tensile component due to the subsequent shrinkage. Therefore, the surface RS of materials with a lower CTE (coefficient of thermal expansion) is more likely to be compressive than those with a higher CTE. Figure 4 plots the surface RS of several austenitic alloys with a different CTE [8]. There is an almost linear relationship between the surface RS and CTE. To clearly demonstrate this relationship, we have applied LPwC conditions that induce tensile RS for a material with a higher CTE, namely SUS304. When the optimum LPwC conditions were applied to these materials, the surface RSs would be sufficiently compressive and close to the yield strengths, so this relationship would not be clear.

Pulse duration is another important parameter affecting the surface RS, as it represents the interaction time of the laser pulse with the material. The shorter the laser pulse,

the smaller the thermal effect. We have therefore developed Nd:YAG lasers with a pulse duration of about 1 ns, which is 1/10 of that of conventional Nd:YAG lasers [9]. This laser dramatically reduces thermal effects in LPwC and can therefore be used without fear of inadvertently inducing tensile RSs [10, 11].

1. A.H. Clauer, *Metals*, **9**, (2019), 626.
2. D.W. See, J.L. Dulaney, A.H. Clauer, and R.D. Tenaglia, *Surf. Eng.*, **18**, (2002), 32.
3. Y. Sano, N. Mukai, K. Okazaki, M. Obata, *Nucl. Instrum. Methods Phys. Res. B*, **121**, (1997), 432.
4. Y. Sano, M. Obata, T. Kubo, N. Mukai, M. Yoda, K. Masaki, Y. Ochi, *Mater. Sci. Eng. A*, **417**, (2006), 334.
5. P. Peyre, L. Berthe, X. Scherpereel, R. Fabbro, *J. Mater. Sci.*, **33**, (1998), 1421.
6. P. Peyre, I. Chaieb, C. Braham, *Modelling Simul. Mater. Sci. Eng.*, **15**, (2007), 205.
7. Y. Sano, K. Akita, T. Sano, *Metals*, **10**, (2020), 816.
8. Y. Sano, K. Akita, *Opt. Laser Technol.*, **156**, (2022), 108528.
9. L. Zheng, A. Kausas, T. Taira, *Opt. Express*, **27**, (2019), 30219.
10. Y. Sano, K. Masaki, Y. Mizuta, S. Tamaki, T. Hosokai, T. Taira, *Metals*, **11**, (2021), 1716.
11. Y. Sano, T. Kato, Y. Mizuta, S. Tamaki, K. Yokofujita, T. Taira, et. al., *Forces Mech.*, **7**, (2022), 100080.

This work was partially supported by the JST-MIRAI Program [grant number JPMJMI17A1] and the Supporting Industry Program of the Small and Medium Enterprise Agency [grant number 20334933]. A part of this work was performed with approval from the Photon Factory Program Advisory Committee of the High-Energy Accelerator Research Organization, Japan (Proposal No. 2003G032 and 2007G082).



KL - 14

EXPERIMENTAL STUDY OF THE VARIATION OF X-RAY ELASTIC CONSTANTS WITH PLASTIC DEFORMATION

P. Faucheux¹, B. Levieil¹, C. Bain¹, L. Barrallier²,

¹ENSTA Bretagne, IRDL—UMR CNRS 6027, 2 Rue François Verny, 29200 Brest, France

²MSMP Arts et Métiers Institute of Technology, HESAM Université, F-13617 Aix-en-Provence, France
bruno.levieil@ensta-bretagne.org

To validate elasto-plastic simulations of complex mechanical parts, it is customary to compare simulated strains to strains measured either using strain gauges or digital image correlation. Alternatively, one can compare simulated stresses to stresses measured by *in-situ* X-ray diffraction. This approach is attractive because it provides direct access to the stresses using only local information from the diffracting volume. However, it requires (i) appropriate diffraction elastic constants to compute stresses from the measured lattice strains and (ii) to deal with intergranular and interphase pseudo-macro stresses that can develop as a result of plastic deformation.

Whereas the evolution of intergranular and interphase micro stresses during plastic deformation has received considerable attention – especially from the neutron and synchrotron communities [1] – fewer studies investigated how diffraction elastic constants vary with plastic strains. Except for a series of articles by Iadicola and co-authors [2], little has been published on that topic since the 1970s (see for example [3-5]). Available experimental data show that depending on the material, processing history, and diffracting planes, diffraction elastic constants can either decrease, remain constant, or increase with plastic deformation, with typical variations of the $1/2 S_2$ constant of about 10%, but sometimes as large as 40% being reported. Failing to take these variations into account results in inaccurate stresses. To the best of our knowledge, robust explanations of this phenomenon are still lacking.

In this contribution, we present some exploratory work that aims at better taking these effects into account when

performing laboratory X-ray stress measurements on uniaxially plastically deformed specimens. In particular, we report a compilation of diffraction elastic constants determined over the 0-2% plastic strain range using a laboratory X-ray diffractometer and a micro-tensile stage that expands data previously reported in [6]. Investigated materials include AISI-1045 steel, 316L steel, 32CrMoV13 steel, high-strength steel, 2017 aluminum, and Ti-6Al-4V. Figure 1 illustrates for a typical subset of results how, for commonly used diffraction conditions, the $1/2 S_2$ constant tends to decrease by 5-10%, the S_1 constant tends to increase by the same amount, and how different surface conditions can result in markedly different diffraction elastic constants.

1. M.T. Hutchings & A.D. Krawitz, *Measurement of residual and applied stress using neutron diffraction*. Springer, 2012.
2. M.A. Iadicola, & T.H. Gnäupel-Herold, *Materials Science and Engineering: A*, (2012), **545**, pp. 168-175.
3. R.. Prümmer, *PhD Thesis*. Universität Karlsruhe, 1967.
4. S. Taira, K. Hayashi, K., Y. Hanayama, *Bulletin of JSME*, **19**, (1970), 196, pp. 49-55.
5. R.H. Marion & J.B. Cohen, *Advances in X-ray Analysis*, **20**, (1976), pp. 355-367.
6. E. Gautier, P. Faucheux, B. Levieil, L. Barrallier, S. Calloch, C. Doudard, *Metals*, **14**, (2024), pp. 62.

Figure 1. Variation of X-ray elastic constants S_1 and $1/2 S_2$ versus plastic strains. Measurements were performed using a Stresstech G2R diffractometer and a micro-tensile stage. Triangle: measurements using a Cr anode of the (211) planes of annealed then electropolished CrMoV13 steel. Crosses: measurements using a Mn anode of the (311) planes of annealed then electropolished 316L steel. Circles: measurements with a Cr anode of the (211) planes of high strength steel with different surface conditions.

KL15

THERMOMECHANICAL FATIGUE OF THIN CU FILMS AT HIGH STRAIN RATES CHARACTERIZED BY 20 KHZ X-RAY DIFFRACTION

T. Ziegelwanger^{1*}, M. Reisinger², K. Hlushko¹, S. Van Petegem³, R. R. Lamas⁴,
M. Meindlhumer¹, J. Todt¹, C. Yildirim⁴, J. Keckes¹

¹Department of Materials Physics, Montanuniversität Leoben, 8700 Leoben, Austria

²KAI Kompetenzzentrum Automobil- u. Industrieelektronik GmbH, 9524 Villach, Austria

³Photons for Engineering and Manufacturing, Paul Scherrer Institute, 5232 Villigen, Switzerland

⁴European Synchrotron Radiation Facility, 38000 Grenoble, France

*tobias.ziegelwanger@unileoben.ac.at

Power electronics face tough challenges in automotive applications posed by high power densities and pulses of $\sim 200 \mu\text{s}$. These pulses heat the device locally above 300°C as common heat dissipation mechanisms via the packaging become ineffective [1]. Currently, thick Cu metallizations are used as heat sinks, but at such small timescales, thermomechanical cycling results in Cu embrittlement. This is not trivial to verify since such short timescales make thermal stress evolution challenging to access experimentally. In this contribution, thermal stresses have been characterized at heating rates of 10^6 K/s using 20 kHz synchrotron X-ray diffraction. Additionally, intragranular 2nd order strain distributions within Cu grains were evaluated using dark-field X-ray microscopy (DFXM).

First, the biaxial thermal stresses of the $20 \mu\text{m}$ thick Cu metallization have successfully been measured at the MS-Powder beamline at Paul Scherrer Institute, Switzerland. A dedicated setup called poly-heater, which can heat chips at a rate of 10^6 K/s , was transferred to the beamline, and in-situ measurements at 20 kHz were performed [2]. Fig. 1a shows results from a representative measurement compared to a wafer curvature experiment of a similar temperature range but at a considerably lower heating rate of 10^{-1} K/s . It is observed that the high strain-rate increased the elastic regime up to 400°C and led to a maximum compressive stress of -391 MPa , which is far more than the -50 MPa observed at lower strain rate. Furthermore, cycling experiments have been performed, showing a decreasing yield

strength of the Cu metallization Fig. 1b. Observations in scanning electron microscopy show that this weakening correlates with the formation of first voids and second cracks in the metallization.

Second, the setup was transferred to the ID06 at the European Synchrotron Radiation Facility in France. Using DFXM, it was possible to image single Cu grains and characterize relevant phenomena such as misorientation and 2nd order intragranular strains. Fig. 2 shows the reconstructed DFXM data from an as-deposited Cu thin film. Fig. 2a shows the mosaicity of the grain and displays a vertical bright blue feature in the center, which is differently oriented from the rest of the grain. In combination with the increased misorientation (Fig. 2b), increased X-ray elastic strain (Fig. 2c), and increased Full width at half maxima (FWHM; Fig. 2d), one can clearly distinguish a twin boundary. These features could be verified via EBSD measurements on the very same grain. In our experiment, thermomechanical cycling between $100\text{--}400^\circ\text{C}$ with $200 \mu\text{s}$ short heating pulses led to increased 2nd order stresses and an increased number of structural defects close to the high-angle grain boundary (HAGB). These findings are the first on thermal strain at such timescales and support existing theories on vacancy condensation at HAGB through partial annihilation of dislocations as a mechanism of fatigue in Cu thin films.

1. M. Nelhiebel et al., "A reliable technology concept for active power cycling to extreme temperatures,"

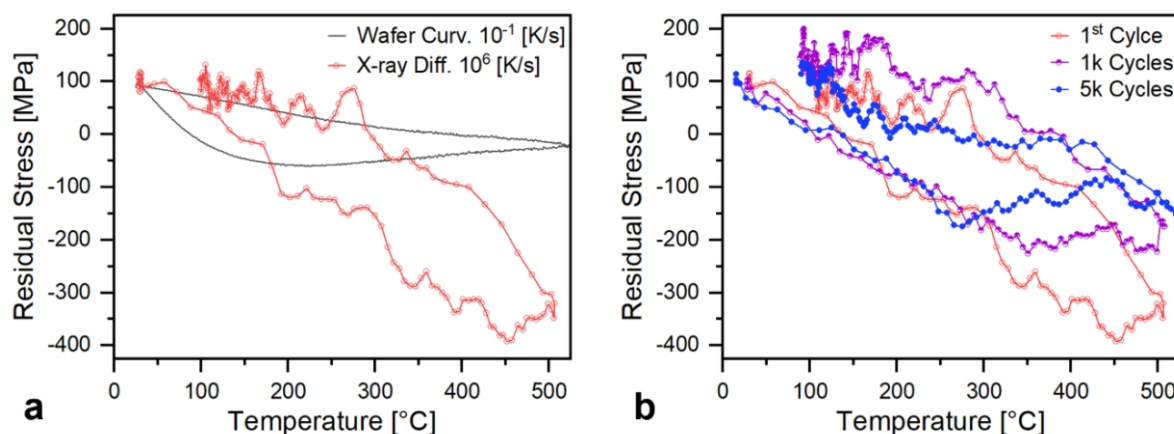


Figure 1. (a) Two stress-temperature diagrams are displayed which were measured at heating rates of 10^{-1} and 10^6 K/s , by wafer curvature and XRD respectively. (b) Up to 5000 periodic heating cycles between $100\text{--}400^\circ\text{C}$ were applied leading to a weakening of the Cu metallization due to fatigue.

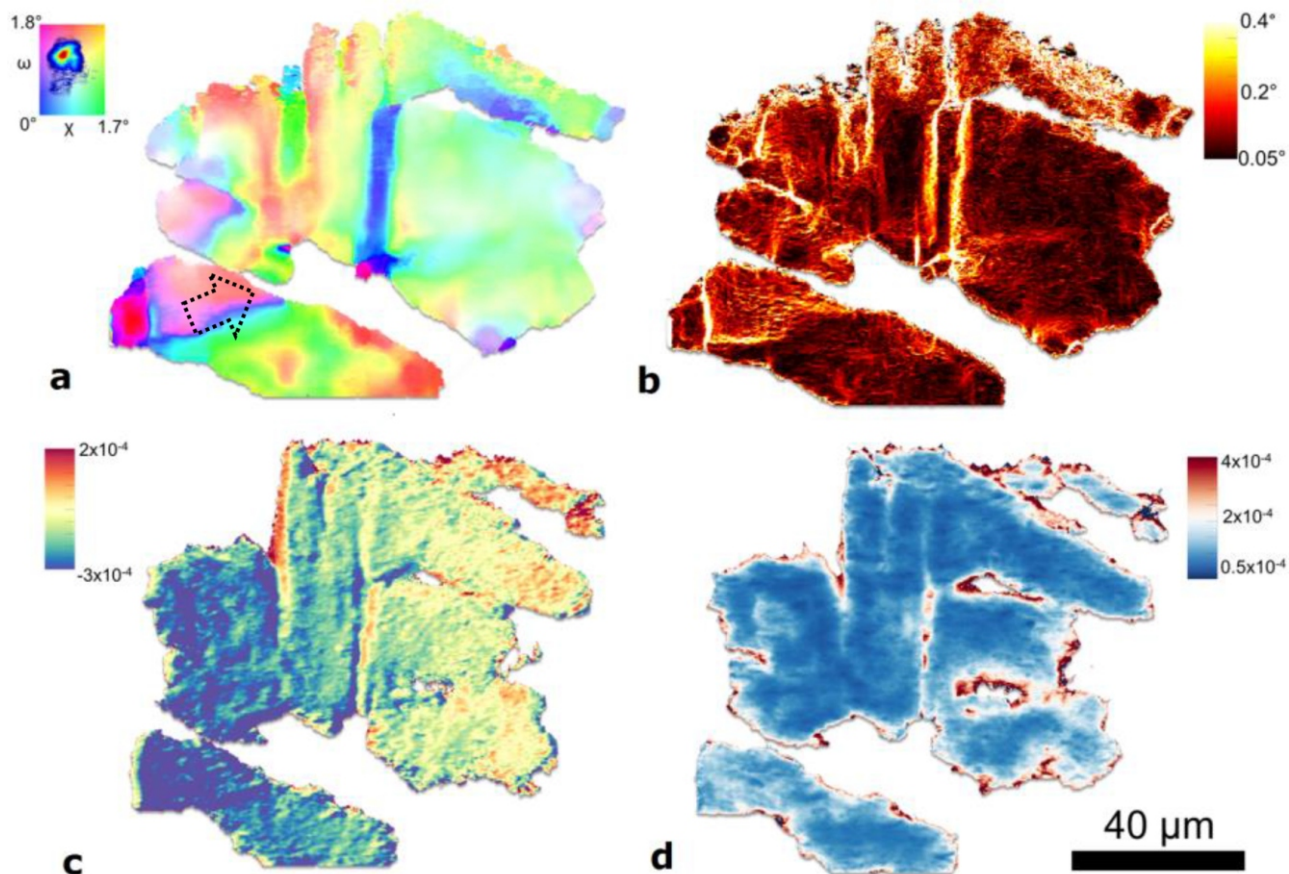


Figure 2. Reconstructed DFXM data from an as-deposited Cu thin film. Displayed are: (a) results from a mosaicity scan, (b) kernel average misorientation, (c) the 2nd order X-ray elastic strains and (d) the FWHM values in degrees [3].

- Microelectron. Reliab., vol. 51, no. 9-11, pp. 1927-1932, Sep. 2011, doi: 10.1016/j.microrel.2011.06.042.
2. S. Moser et al., "A Novel Setup for In Situ Monitoring of Thermomechanically Cycled Thin Film Metallizations," JOM, vol. 71, no. 10, pp. 3399-3406, Oct. 2019, doi: 10.1007/s11837-019-03695-2.
 3. K. Hlushko et al., "Intragranular thermal fatigue of Cu thin films: Near-grain boundary hardening, strain localization and voiding," Acta Mater., vol. 253, p. 118961, Jul. 2023, doi: 10.1016/j.actamat.2023.118961.

KL16

BETWEEN NEUTRONS AND X-RAYS, AN OVERVIEW OF THE HIGH ENERGY WHITE BEAM BEAMLINE P61A @ PETRA III

G. Abreu Faria, M.-A. Nielsen, P. Staron, M. Mueller

*Helmholtz-Zentrum hereon, Notkestraße 85, Hamburg, Germany
Guilherme.abreu@hereon.de*

High energy synchrotron X-ray diffraction (SXR) is instrumental in the high spatial resolution measurement of strain fields. Although the high energies enable measurement of parts up to a few centimetre thick, when SXR is performed with a monochromatic beam in angle dispersive geometry, information is averaged through the thickness of the part. This makes it disadvantageous in the measurement of large parts, as these must be sectioned, therefore changing the stress state. Non-destructive characterization of large parts require the definition of a Gauge Volume (GV) inside of the part, as done with neutrons. GV definition can be done with angle dispersive SXR using conical slits, but this comes at the expense of the measured q range. In contrast, Energy Dispersive (ED) SXR uses point detectors, which still measure the full q -range. By collimating the scattered beam, it is possible to define a GV inside of the sample. If a high flux at high energies is available, measurements can be performed with fast data collection, high spatial resolution, and GV control.

This work reports on the dedicated white beam beamline P61A. P61A is active since 2021, and is operated by hereon at the PETRA III synchrotron. Its incident beam is supplied by a unique insertion device: an array of ten 4 m long damping wigglers. These yield a high flux continuous

beam with usable energies up to 200 keV. The beamline is equipped with several ED detectors which can be positioned to measure different strain components. Each detector is equipped with collimating slits allowing for GV adjustment during an experiment. Heavy load sample positioning devices are available, including a 20 kg load capacity Eulerian cradle, enabling \sin^2 or strain pole figure measurements. P61A's characteristics make it ideal for stress determination experiments. GVs of $0.05 \times 0.05 \times 0.75 \mu\text{m}^3$ can be achieved, and measurements in up to 40 mm thick steel samples have been performed. As an instrument, P61A's performance fits the niche between neutron and high energy monochromatic SXR beamlines, delivering high spatial resolution, short acquisition times and the ability to measure through centimetre thick parts. The white beam brings another advantage: when measurements are done in reflection geometry, near surface stress gradients can be determined by the use of Laplace space methods. At P61A, stress gradients can be determined through depths down to 250 μm thick in steels.

This presentation will cover the beamline key instrumentation and performance figures, including examples of stress determination experiments carried out so far.